The Astrophysical Journal, 778:149 (27pp), 2013 December 1 doi:10.1088/0004-637X/778/2/149

CHEMISTRY OF THE SAGITTARIUS DWARF GALAXY: A TOP-LIGHT INITIAL MASS FUNCTION, OUTFLOWS, AND THE *R*-PROCESS

Andrew McWilliam[1], George Wallerstein[2], and Marta Mottini[2]
[1] The Observatories of the Carnegie Institute of Washington, 813 Santa Barbara Street, Pasadena, CA 91101, USA; andy@obs.carnegiescience.edu
[2] Astronomy Department, University of Washington, Seattle, WA 98195, USA; walleg@u.washington.edu
Received 2013 July 5; accepted 2013 September 9; published 2013 November 12

ABSTRACT

From chemical abundance analysis of stars in the Sagittarius dwarf spheroidal galaxy (Sgr), we conclude that the α-element deficiencies cannot be due to the Type Ia supernova (SN Ia) time-delay scenario of Tinsley. Instead, the evidence points to low [α/Fe] ratios resulting from an initial mass function (IMF) deficient in the highest mass stars. The critical evidence is the 0.4 dex deficiency of [O/Fe], [Mg/Fe], and other hydrostatic elements, contrasting with the normal trend of *r*-process [Eu/Fe]$_r$ with [Fe/H]. Supporting evidence comes from the hydrostatic element (O, Mg, Na, Al, Cu) [X/Fe] ratios, which are inconsistent with iron added to the Milky Way (MW) disk trends. Also, the ratio of hydrostatic to explosive (Si, Ca, Ti) element abundances suggests a relatively top-light IMF. Abundance similarities with the LMC, Fornax, and IC 1613 suggest that their α-element deficiencies also resulted from IMFs lacking the most massive SNe II. The top-light IMF, as well as the normal trend of *r*-process [Eu/Fe]$_r$ with [Fe/H] in Sgr, indicates that massive SNe II ($\gtrsim$30 $M_\odot$) are not major sources of *r*-process elements. High [La/Y] ratios, consistent with leaky-box chemical evolution, are confirmed but $\sim$0.3 dex larger than theoretical asymptotic giant branch (AGB) predictions. This suggests that a substantial increase in the theoretical ^{13}C pocket in low-mass AGB stars is required. Sgr has the lowest [Rb/Zr] ratios known, consistent with pollution by low-mass ($\lesssim$2 $M_\odot$) AGB stars near [Fe/H] = $-$0.6, likely resulting from leaky-box chemical evolution. The [Cu/O] trends in Sgr and the MW suggest that Cu yields increase with both metallicity and stellar mass, as expected from Cu production by the weak *s*-process in massive stars. Finally, we present an updated hyperfine splitting line list, an abundance analysis of Arcturus, and further develop our error analysis formalism.

Key words: galaxies: abundances – galaxies: dwarf – stars: abundances – stars: late-type

Online-only material: color figures, machine-readable tables

1. INTRODUCTION

The Sagittarius dwarf Spheroidal galaxy (Sgr), which is merging with the Milky Way (MW), has six associated globular clusters: Ter 7, Pal 12, Whiting 1, M54, Arp 2, and Ter 8. The first three clusters are middle-aged (6–8 Gyr) and metal-rich, with [Fe/H] between $-$0.6 and $-$0.8 dex, while the last three are old (11–14 Gyr) and metal-poor, with [Fe/H] in the range $-$1.6 to $-$2.3 dex. M54 (=NGC 6715), the most populous cluster, lies in the densest part of Sgr (Ibata et al. 1994; Sarajedini & Layden 1995; Monaco et al. 2005). This has prompted discussion of whether M54 is the nucleus of the Sgr galaxy (Sarajedini & Layden 1995; Da Costa & Armandroff 1995; Layden & Sarajedini 2000), around which later star formation occurred.

Ground-based photometric observations by Sarajedini & Layden (1995) and Layden & Sarajedini (2000) and *Hubble Space Telescope* photometry of M54 by Siegel et al. (2007) show that M54 contains a second, fainter red giant branch (RGB). Analysis by Siegel et al. (2007) indicated an old (13 Gyr) population with the presence of at least two intermediate-aged populations: 4–6 Gyr with [Fe/H] = $-$0.4 to $-$0.6 dex, from the fainter RGB, and a 2.3 Gyr population near solar abundance. These observations may indicate that M54 has two, or more, populations with significantly different [Fe/H], making it an unusual globular cluster, similar to ω Cen. The density of stars in the faint RGB Sgr population is larger in the central M54 field than the Sgr field, studied by Layden & Sarajedini (2000), which suggests the possibility that the faint RGB stars belong to a late episode of star formation within the globular cluster, rather than the Sgr galaxy itself. Monaco et al. (2005) found a strong density enhancement in Sgr, with a peak that is indistinguishable from the center of M54; they concluded that Sgr is a nucleated dwarf galaxy, even when M54 is ignored.

However, Siegel et al. (2007) claim that the fainter RGB belongs to Sgr, and that it is possible that M54 formed separately from Sgr's nucleus and was later pulled into the galaxy's center through dynamical friction.

A spectroscopic study by Bellazzini et al. (2008) found that the velocity dispersion of the faint RGB is identical to that of Sgr, which is constant from 0.5 arcmin out to at least 100 arcmin from M54. This constant velocity dispersion for Sgr, at 9.6 km s^{-1}, over an extended region, much larger than M54, is strong evidence supporting the idea that the faint RGB in M54 is part of the Sgr galaxy, rather than the globular cluster. This differs from the velocity dispersion trend in M54, which declines from 14.2 km s^{-1} at the center to $\sim$5.0 km s^{-1} at a distance of 3.5 arcmin.

Bellazzini et al. (2008) also found a bimodal metallicity function, based on Ca-triplet measurements, one peaked at [Fe/H] = $-$1.45 and the other at [Fe/H] = $-$0.45, in good agreement with but $\sim$0.1 dex higher than other metallicity estimates for the main body of M54 and Sgr, respectively. Thus, Bellazzini et al. (2008) showed that the faint RGB toward M54 is, in fact, due to Sgr.

Several photometric and spectroscopic studies of M54 have been undertaken, providing information on the cluster's characteristics (distance, reddening, etc.) and estimates of the metallicity. Sarajedini & Layden (1995) found [Fe/H] = $-$1.79 $\pm$ 0.08 from photometry of RGB stars and an intrinsic dispersion of 0.16 dex. Da Costa & Armandroff (1995) estimated M54's metallicity from the Ca II triplet, assuming that the [Ca/Fe]

Table 1
Observations

Star	R.A. (2000)	Decl. (2000)	V	Exp. (s)	S/N	RV_{helio}
242	18:55:17.9	−30:27:49	16.225	5700	39	145.4
247	18:54:48.3	−30:26:39	16.241	8100	50	145.4
266	18:54:40.5	−30:26:49	16.292	6000	42	131.8

Notes. Star identifications and V magnitudes are from the shallow M54 frame data of Layden & Sarajedini (2000). The S/N values are final, per extracted pixel, at the peak of the Hα order.

ratio is similar to normal metal-poor stars, and found [Fe/H] = −1.55 ± 0.10 dex. Sarajedini & Layden (1997) discussed the systematic effects on metallicity estimates from photometry and Ca II triplet spectroscopy in the case of non-standard [α/Fe] ratios.

The first high-resolution model atmosphere abundance analysis of M54 stars was undertaken by Brown et al. (1999). They studied five red giants belonging to the bright, or main, RGB of M54 and found [Fe/H] = −1.55 ± 0.10 dex, with oxygen and other α-elements characteristic of the MW halo.

From Two Micron All Sky Survey (2MASS) photometry of stars in the Sgr RGB, Cole (2001) found a mean [Fe/H] of −0.5 ± 0.2 dex. Detailed, high-resolution abundance studies of Sgr stars include Bonifacio et al. (2000, 2004, henceforth B00, B04), Smecker-Hane & McWilliam (2002, henceforth SM02), Sbordone et al. (2007, henceforth S07), and Carretta et al. (2010, henceforth C10). These studies found [Fe/H] for individual Sgr stars, ranging from below −1 to above solar. In their study, C10 found [Fe/H] = −1.56 dex for M54, based on 76 stars, and a mean [Fe/H] = −0.62 for Sgr from 27 stars.

In this paper we discuss a detailed chemical abundance analysis of three red giant stars belonging to the fainter RGB toward M54, which Bellazzini et al. (2008) found to be kinematic members of Sgr. We compare our results to previous abundance studies of Sgr, in order to understand the complex chemical evolution of this system.

In Section 2 we describe our observations and the data reduction, in Section 3 we describe the abundance analysis procedures, and we discuss our findings and conclusions in Sections 4–6.

2. OBSERVATIONS AND DATA REDUCTION

We acquired high-resolution spectra of three stars on the fainter giant branch of M54 in 2007 July. Target selection employed the color–magnitude diagrams and finding chart for the M54 shallow frames of Layden & Sarajedini (2000). The stars were chosen to be relatively bright ($V \sim 16.2$) and isolated, with colors indicating that these were late K-type giants, not M giants. This was important, because the TiO absorption present in M giants would have made the abundance analysis significantly more difficult.

The spectra were obtained using the Magellan Echelle spectrograph, MIKE, with a 0.5 arcsec slit, corresponding to $R \sim$ 48,000. Typical exposure times were 6000 s, resulting in signal-to-noise ratio (S/N) values near 40 at the peak of the Hα order; actual exposure times and final, per extracted pixel, S/N values are listed in Table 1. Due to line crowding and reduced S/N toward the blue, the portion of our spectra useful for abundance analysis ranged from 5120 to 9250 Å.

The spectra were reduced using the MIKE pipeline, written by Dan Kelson (see Kelson 2003 for details). In order to flatten the spectra, we traced the continuum of a hot star, HR 9098 (B9IV), from a high-S/N spectrum obtained in the same observing run as the M54/Sgr stars. The continuum fit for this *blaze standard* was performed using the IRAF *continuum* routine, with a high-order cubic spline fit.

3. ABUNDANCE ANALYSIS

Radial velocities of our three stars were determined by measuring the central wavelengths of a handful of strong lines in the spectra. Conversion to heliocentric velocities was accomplished using the IRAF *rvcorrect* algorithm; the results are listed in Table 1.

The mean heliocentric velocities of our three stars are +140.9 ± 4.6 km s^{-1}. This value is consistent with measurements of the mean heliocentric velocities of both the M54 core and the Sagittarius nucleus, at +140.7 ± 0.4 and +139.9 ± 0.6 km s^{-1}, respectively (see Bellazzini et al. 2008). The velocity dispersion of our stars, at $\sigma = 7.9$ km s^{-1}, is also consistent with the constant value of $\sigma = 9.6$ km s^{-1} for Bellazzini's Sagittarius nucleus and their positions in the color–magnitude diagram.

In this work we employ equivalent width (EW) model atmosphere abundance analysis for most elements; however, spectrum synthesis profile matching calculations were used to determine abundances in a few cases where critical lines were blended or partially blended. The lines used here for abundance analysis were selected from a number of our previous papers on abundances in red giant stars, including Fulbright et al. (2007), Koch & McWilliam (2008), SM02, and McWilliam et al. (1995). We also include a number of new lines identified as potentially useful in this work, in particular Rb I λ7948 and the Zr I lines at 8070, 8133, and 8389 Å.

Because of the relatively low S/N of our spectra, especially at bluer wavelengths, the lines we have used tend to be near the flux peaks of the echelle orders, where relatively weak lines can be reliably measured.

Our line EWs were measured from the flattened spectra by A.M. and G.W., independently, using the IRAF *splot* routine. To identify continuum regions and for blend detection, the high-quality spectral atlas of Arcturus (Hinkle et al. 2000) was particularly useful. The final, average EWs for the lines used in this paper are listed in Table 2.

The abundance analysis follows the differential method, relative to Arcturus, we devised in Fulbright et al. (2007) and employed by Koch & McWilliam (2008, 2010, 2011). We use the spectrum synthesis program MOOG (Sneden 1973) and Kurucz's model atmospheres from his Web site, at http://kurucz.harvard.edu, as discussed in Castelli et al. (1997).

Line-by-line differential abundance studies possess several advantages that improve the accuracy of abundance measurement, particularly when the target and standard star are of similar spectral type. For example, the accuracy of the gf values becomes unimportant, thus allowing lines with poorly measured or unknown gf values to be used. Even the effects of unidentified line blends should be reduced when taking differential abundances, relative to a similar standard star.

Unaccounted effects in the model atmospheres, such as three-dimensional (3D) hydrodynamics, granulation, non-LTE, and the effect of a chromosphere on the T–τ relation, are likely to be very similar in standard and target stars, provided that the atmosphere parameters are close enough. However, no calculations yet exist to show how similar the program and standard stars need to be for good cancellation of systematic

Table 2
Line List

Ion	λ	E.P.	Star 242		Star 247		Star 266		Notes
	(Å)	(eV)	EW	$\Delta\varepsilon_{aboo}$	EW	$\Delta\varepsilon_{aboo}$	EW	$\Delta\varepsilon_{aboo}$	
[O I]	6300.30	0.00	60	−0.46	61	−0.23	63	−0.40	ss,ew
Na I	6154.23	2.10	68	−0.41	80	−0.22	75	−0.30	
Na I	6160.75	2.10	80	−0.60	86	−0.37	98	−0.22	
Mg I	5711.09	4.35	136	−0.51	137	−0.20	140	−0.37	
Mg I	6318.77	5.11	46:	−0.45	52:	−0.23:	...	...	
Mg I	6319.24	5.11	34	−0.42	40	−0.21	28:	−0.53:	
Mg I	8717.82	5.93	56	−0.45	64	−0.14	52	−0.49	
Mg I	8736.02	5.96	94	−0.44	119	+0.17	100	−0.32	

(This table is available in its entirety in a machine-readable form in the online journal. A portion is shown here for guidance regarding its form and content.)

Table 3
Arcturus Abundance Ratios

Ion	[X/Fe]	σ	N_{lines}
[Fe I/H]	−0.49	0.07	152
[Fe II/H]	−0.40	0.04	8
[O I][a]	+0.46	...	1
Na I	+0.09	...	1
Mg I	+0.39	0.06	5
Al I	+0.38	0.03	3
Si I	+0.35	0.05	15
Ca I	+0.21	0.01	2
Ti I	+0.26	0.04	17
Ti II[a]	+0.26	0.04	7
V I[b]	+0.12	0.02	3
Mn I[b]	−0.14	0.09	4
Cu I[b]	+0.30	...	1
Rb I[b]	+0.05	0.01	2
Zr I[b]	−0.28	0.09	3
Y II[a, b]	−0.22	0.14	6
Ba II[a]	−0.17	...	1
La II[a, b]	−0.08	0.09	6
Eu II[a, b]	+0.23	0.06	2
[α/Fe]	+0.32	0.09	6[c]

Notes. Note that sigmas only reflect the dispersion within the line list for each species and do not include systematic errors.
[a] Relative to Fe II.
[b] hfs treatment employed to compute abundances.
[c] Number of elements used to compute [α/Fe].

errors. On the other hand, so long as the model atmosphere abundance corrections from the various unaccounted physical effects have the same sign in the program and standard stars, then the differential abundances should be more reliable than the absolute model atmosphere abundances.

While use of the Sun as a differential standard would always eliminate the gf value problem, Arcturus should be a superior differential standard for our Sgr RGB target stars. In particular, we can use lines that are present in Arcturus and our Sgr RGB stars that are not detected in the solar spectrum (e.g., Rb I λ7948 and Zr I lines at 8070, 8133, and 8389 Å).

However, to use Arcturus as a standard requires that we have an accurate measurement of its chemical abundance distribution, relative to the Sun. Fortunately, an extremely high quality spectrum of Arcturus, from UV to IR, is available (i.e., Hinkle et al. 2000), matching the quality of the Kurucz et al. (1984) solar spectrum. Thanks to the proximity of Arcturus, its atmosphere parameters are known to a precision better than any other RGB star (see Fulbright et al. 2007; Koch & McWilliam 2008).

In this work we increase the number of elements in Arcturus with differential abundance ratios, [X/Fe], relative to the Sun, using the same Arcturus model atmosphere as Koch & McWilliam (2008). The adopted abundance ratios are presented in Table 3.

3.1. Hyperfine and Isotopic Splitting

For most species we employed the single-line, EW, line-by-line, differential abundance analysis, relative to Arcturus. However, the lines of a number of elements studied here suffer from de-saturation due to hyperfine splitting (hereafter hfs) and/or isotopic splitting. For these elements it was necessary to include the fine-structure components in the spectrum synthesis calculations. Where possible, we employed hfs lists that we had previously employed or calculated in other studies, but for a few lines we searched the literature for the latest hfs and isotopic splitting constants. Thus, our hfs line lists are the best available for several lines, in particular the Rb I and Zr I lines. The hfs energy level splittings were computed using Equations (1) and (2), below. For Cu, Rb, Zr, and Eu we adopted solar isotopic compositions in the line lists. Table 4 in the electronic version shows the complete hfs and isotopic line lists used in this work; a table of hfs references for each species is also provided:

$$\Delta E = \frac{1}{2}AK - B\frac{\frac{3}{4}K(K+1) - J(J+1)I(I+1)}{2I(2I-1)J(2J-1)}, \quad (1)$$

where

$$K = F(F+1) - I(I+1) - J(J+1). \quad (2)$$

Here, I is the nuclear angular momentum quantum number for the isotope, J is the total electronic quantum number for the level, F is the total angular momentum quantum number for the atom in a given hyperfine level (F is the vector sum of the nuclear and electronic momenta), and A and B are the hyperfine constants. The relative strengths of the levels are computed according to Condon & Shortly (1935, page 238). Also, see Woodgate (1980) for a useful discussion. We also recommend Johnson et al. (2006) as a resource for hfs line lists.

3.2. Model Atmosphere Parameters

Our stellar atmosphere parameters were determined using the *VI* photometry of Layden & Sarajedini (2000) and the *JHK* 2MASS data from Skrutskie et al. (2006). Reddening corrections were based on the extinction relations of Winkler

Table 4
hfs List

Species	Wavelength (Å)	log $F_i gf$
^{87}Rb I	7800.2480	−1.2181
^{87}Rb I	7800.2515	−1.2181
^{87}Rb I	7800.2529	−1.6160
^{85}Rb I	7800.2993	−0.8855
^{85}Rb I	7800.3008	−0.7886
^{85}Rb I	7800.3013	−0.9013
^{85}Rb I	7800.3584	−0.4241
^{85}Rb I	7800.3608	−0.7886
^{85}Rb I	7800.3623	−1.3326
^{87}Rb I	7800.3813	−0.7709
^{87}Rb I	7800.3867	−1.2181
^{87}Rb I	7800.3901	−1.9171
^{87}Rb I	7947.5747	−1.2249
^{87}Rb I	7947.5918	−1.9239
^{85}Rb I	7947.6323	−0.7954
^{85}Rb I	7947.6401	−1.3395
^{85}Rb I	7947.6963	−0.8923
^{85}Rb I	7947.7041	−0.7954
^{87}Rb I	7947.7188	−1.2249
^{87}Rb I	7947.7358	−1.2249

Notes. F_i indicates isotopic fraction.

(This table is available in its entirety in a machine-readable form in the online journal. A portion is shown here for guidance regarding its form and content.)

(1997), with $E(B-V) = 0.15$, adopted from Siegel et al. (2007). Color temperatures were based on the calibration of Ramírez & Meléndez (2005, henceforth RM05), assuming [Fe/H] = −0.5. This temperature scale is similar to other currently popular calibrations: the Casagrande et al. (2010) scale is hotter than RM05 by 40 K; RM05 is hotter than Alonso et al. (1999) by 18 K. The physical temperature for Arcturus, from Fulbright et al. (2006), is 4290 K, with a 1σ uncertainty of ±29 K (Koch & McWilliam 2008, henceforth KM08).

The Lee (1970) and Johnson et al. (1966) photometry of Arcturus gives $(V-I)_J$, $(V-J)_J$, and $(V-K)_J$ of 1.62, 2.08, and 2.925 mag. respectively. Note that the 2MASS *JHK* photometry for Arcturus is highly uncertain, with 1$\sigma \sim 0.17$ mag, likely due to saturation effects, and therefore not used. Transformation of the Johnson $(V-I)$ color to the Kron-Cousins system is accomplished by use of the relations in Bessell (1979). Transformation of the Johnson $(V-J)$ and $(V-K)$ colors to the K-short system used by 2MASS was obtained by first converting from the Johnson to CIT system with the relations of Elias et al. (1985) and then to the 2MASS system with the relations given by Carpenter (2005, unpublished).[3]

[3] http://www.astro.caltech.edu/~jmc/2mass/v3/transformations/

Table 6
Adopted Model Atmosphere Parameters

Star	$T_{\rm eff}$	log g	[A/H]	ξ	[Fe I/H]$_{\rm lines}$
242	3920	0.96	−0.5	1.7	−0.49
247	3850	0.83	−0.2	1.4	−0.09
266	3920	0.93	−0.5	1.6	−0.39
Arcturus	4290	1.60	−0.5	1.6	−0.49

Notes. Gravities were found using the adopted $T_{\rm eff}$ values and a 5 Gyr (recommended by Siegel et al. 2007) Teramo canonical, scaled-solar composition isochrone with $z = 0.008$. For log g determination stars were assumed to be on the RGB; log g for AGB stars would have been 0.07 dex smaller. Note that the observed M_v for star 242 is closer to the AGB value than the RGB value in the Teramo isochrone.

We find that the RM05 $V-K$ calibration gives $T_{\rm eff}$ for Arcturus of 4275 K, some 15 K cooler than the physical effective temperature; this is well within the uncertainties on the physical $T_{\rm eff}$ and corresponds to a mere 0.023 mag error in the $V-K$ color. Therefore, we have adopted the RM05 photometric temperature calibration for this work. Table 5 summarizes the photometry and resultant temperatures for each color, based on the RM05 calibrations and [Fe/H] = −0.5; we also include the transformed colors and color temperatures derived for Arcturus, showing good agreement with the physical $T_{\rm eff}$.

Photometric gravities were found using the adopted $T_{\rm eff}$ values and a 5 Gyr (recommended by Siegel et al. 2007) Teramo canonical, scaled-solar composition isochrone with $z = 0.008$. We assumed that our stars are on the RGB; log g for asymptotic giant branch (AGB) stars would have been 0.07 dex smaller.

As usual, we iterated on the microturbulent velocity, metallicity, and [α/Fe] enhancement. The microturbulent velocities were chosen by requiring that Fe I abundances be independent of EW.

Once the [Fe/H] derived from iron lines and model metallicity were roughly consistent, we computed the mean [α/Fe] from our abundances of O, Mg, Si, Ca, and Ti, which we employed to select the appropriate [α/Fe] ratio of the model atmospheres for the abundance analysis. The use of model atmospheres with the appropriate [α/Fe] ratio is necessary due to the contribution of free electrons from the ionization of Mg and Si, which in turn affects the H^- continuous opacity and computed line strengths, particularly for lines from species of the dominant ionization stage (e.g., O I, Fe II, La II). Since our results show [α/Fe] near zero, and below, for all three program stars, we have adopted the scaled solar composition Kurucz model atmospheres. Future analyses might consider use of sub-solar [α/Fe] model atmospheres for Sgr stars. Our final adopted model atmosphere parameters are listed in Table 6.

Table 5
Photometry and Temperatures

Star	V	$(V-I)_0$	$(V-J)_0$	$(V-K)_0$	$T(V-I)$	$T(V-J)$	$T(V-K)$	$\overline{T}_{\rm eff}$
242	16.225	1.604	2.707	3.663	3921	3916	3922	3920
247	16.241	1.676	3.050	3.728	3873	3787	3897	3852
266	16.292	1.642	2.722	3.615	3895	3909	3941	3915
Arcturus	−0.05	1.260	2.137	2.940	4272	4283	4275	

Notes. De-reddened optical, V, and Kron-Cousins I-band photometry, from Layden & Sarajedini (2000), and infrared photometry from the 2MASS catalog (Skrutskie et al. 2006). Reddening corrections were based on Winkler (1997), with $E(B-V) = 0.15$, adopted from Siegel et al. (2007). Arcturus colors transformed from Lee (1970) and Johnson et al. (1966); see the text. Color temperatures were based on the calibration of Ramírez & Meléndez (2005), assuming [Fe/H] = −0.5.

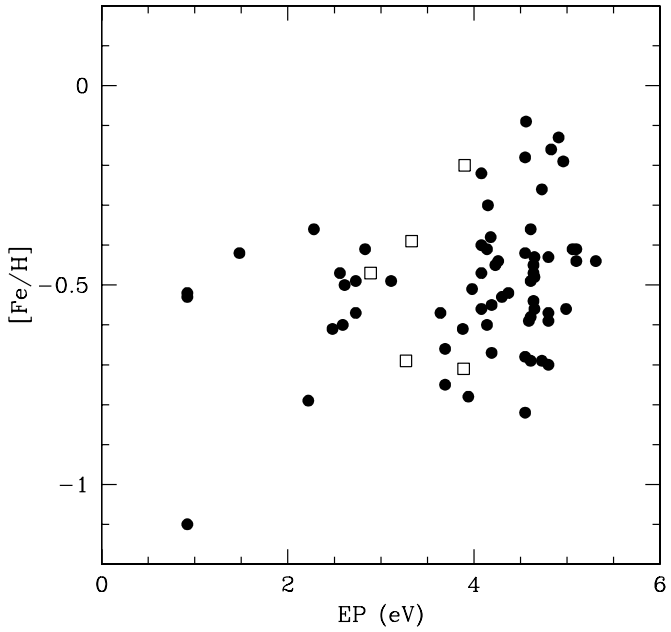

Figure 1. Star 242 [Fe/H] vs. excitation potential, in eV, for differential line-by-line Fe I (filled circles) and Fe II (open squares) abundances. The lack of a strong slope indicates consistency of the line excitation with the adopted model atmosphere $T_{\rm eff}$, determined photometrically. Note that ionization equilibrium is obtained.

A check on our photometric temperatures is obtained from a plot of differential Fe abundance versus line excitation potential, as shown in Figure 1. We note that our Arcturus [Fe I/H] and [Fe II/H] values, taken line by line relative to the Sun, are −0.49 and −0.40, respectively, a result similar to that found by Koch & McWilliam (2008). The ionization imbalance might be due to improper accounting for the electron number density, such as might occur with erroneous [α/Fe], incorrect adopted gravity, non-LTE over-ionization of Fe I, or other difficulties. For our stellar [Fe I/H] and [Fe II/H] abundances we are ultimately referenced to the Sun, so the Arcturus zero point does not affect our results. For ionized species in the program stars, we take the [X II/Fe II] ratios, which cancels out the Arcturus zero-point offset in Fe II.

In principle, it should be possible to check the adopted gravity of our program stars from ionization equilibrium of Fe and Ti, since Fe II and Ti II lines are sensitive to the electron density in the atmosphere, which is strongly affected by gravity. Unfortunately, the large dispersion of our measured Ti II abundances excludes this element for use as a gravity discriminator. For iron we note that while star 242 shows excellent agreement between Fe I and Fe II abundances, the Fe II abundances are 0.11 and 0.13 dex higher than Fe I in stars 247 and 266, respectively. The excess Fe II abundances could, reasonably, be due to measurement error. It cannot result from these two stars being on the AGB rather than the RGB, since the small gravity change, of 0.07 dex, leads to an abundance difference of only 0.03 dex (see Table 9 in Appendix A); thus, a much larger gravity difference is required to explain the apparent difference between Fe I and Fe II abundances. An alternative explanation, perhaps more realistic, for the ionization imbalance is that the electron density, N_e, in stars 247 and 266 is significantly lower than expected from the scaled solar model atmospheres employed due to the large underabundances of Na, Mg, Al, and Si (see Table 7); these elements are important electron donors in the atmospheres of our stars. A calculation of N_e for two locations in the line-forming region of the model atmosphere for star 266 showed that the measured abundance deficiencies of O, Na, Mg, Al, Si, Ca, and Ti lead to a reduction of N_e by ∼30%, or ∼0.1 dex, roughly consistent with the putative ionization imbalance. Other possible explanations for the apparent ionization imbalance include excessive mass loss in the program stars, leading to lower than expected gravity, and strongly enhanced He abundances.

Table 7
Abundance Results

	242			247			266		
Ion	[X/Fe]	σ	N	[X/Fe]	σ	N	[X/Fe]	σ	N
[Fe I/H]	−0.49	0.18	64	−0.09	0.19	65	−0.39	0.22	56
[Fe II/H]	−0.47	0.21	5	+0.02	0.12	5	−0.26	0.18	3
[O I][a]	−0.02	···	1	−0.19	···	1	−0.04	···	1
Na I	−0.43	0.13	2	−0.63	0.11	2	−0.28	0.06	2
Mg I	−0.07	0.03	5	−0.14	0.17	5	−0.15	0.10	4
Al I	−0.09	0.07	5	−0.31	0.09	5	−0.09	0.12	2
Si I	−0.08	0.16	7	+0.00	0.16	9	+0.08	0.22	9
Ca I	+0.01	0.16	6	−0.17	0.16	4	+0.09	0.15	5
Ti I	−0.08	0.18	9	−0.09	0.18	9	−0.02	0.14	9
Ti II[a]	+0.00	0.20	2	−0.06	0.16	2	−0.14	0.37	2
V I[b]	−0.08	0.08	3	−0.06	0.02	3	+0.09	0.10	3
Mn I[b]	−0.27	0.08	4	−0.06	0.10	4	−0.03	0.05	4
Cu I[b]	−0.64	···	1	−0.31	···	1	−0.44	···	1
Rb I[b]	−0.19	0.01	2	−0.44	0.06	2	−0.21	0.02	2
Zr I[b]	−0.08	0.10	6	+0.28	0.07	6	+0.08	0.08	6
Y II[a, b]	−0.20	0.10	5	−0.39	0.20	5	−0.08	0.13	5
La II[a, b]	+0.49	0.16	4	+0.48	0.23	4	+0.40	0.10	4
Eu II[a, b]	+0.39	···	1	+0.23	···	1	+0.32	···	1
α/Fe	−0.04	0.04	6	−0.11	0.07	6	−0.03	0.10	6
log ϵ(Li)[c]	+0.42	···	1	+0.14	···	1	−0.47	···	1

Notes. Note that sigmas indicate the rms dispersion of the measurements for species with more than one line; they are dispersions, not errors on the mean.
[a] Relative to Fe II.
[b] hfs/EW treatment employed to compute abundances.
[c] Absolute abundances listed for Li, based on the line list of Andersen et al. (1984).

4. ABUNDANCE RESULTS AND DISCUSSION

Abundance results for our three Sgr stars are provided in Table 7. In this table we list the [Fe/H] derived from Fe I and Fe II lines separately; we also show element-to-iron ratios, [X/Fe], where the normalizing iron abundance (Fe I or Fe II) is chosen to minimize the effects of systematic errors in the atmosphere parameters. For lithium only, Table 7 provides the absolute lithium abundances on the hydrogen = 12.0 scale, ϵ(Li); the abundances are based on the hfs line list of Andersen et al. (1984) and are *not* differential to any standard star.

4.1. Iron

The [Fe/H] values for our three stars, 242, 247, and 266, are −0.49, −0.09, and −0.39 dex, respectively. The dispersion of these [Fe/H] values is too large to be due to measurement error about a single mean value for Sgr. Our formal best estimate for the internal 1σ [Fe/H] measurement uncertainty is 0.03 dex (see Table 11 in Appendix A), while our most pessimistic estimate of this internal [Fe/H] uncertainty, within our sample, is 0.10 dex. The reduced Chi-squared fit assuming a single [Fe/H] value is $\chi^2 \sim 48$ for the former measurement error, and $\chi^2 \sim 4$ for the pessimistic 0.10 dex measurement uncertainty. Thus, we

conclude that our measurements are best represented with a 1σ intrinsic abundance spread, near 0.20 dex, about the mean of [Fe/H] = −0.32 dex. The conclusion that our reported [Fe/H] differences are real is supported by the systematic difference in line EWs between the three stars, even though the stellar temperatures are similar.

The [Fe/H] values of our three stars are consistent with the mean values and ranges of photometric and spectroscopic metallicities reported for Sgr from a number of studies: Cole (2001), SM02, S07, Siegel et al. (2007), Bellazzini et al. (2008), B00, B04, and C10. These studies show a consistent picture, with Sgr stars ranging in [Fe/H] from near −1 to above the solar value, with a mean at approximately −0.5 dex.

While the mean [Fe/H] and [Fe/H] dispersion found here are consistent with the results of previous Sgr studies, our selection of stars from the faint RGB, below the M54 giant branch, has biased us to the mean and more metal-rich side of the Sgr metallicity distribution.

4.2. The α-Elements

Wallerstein (1962) discovered that metal-poor, MW halo stars showed excesses of Mg, Si, Ca, and Ti, relative to Fe; later, Conti et al. (1967) found similar excesses for O. These even-numbered elements (O, Mg, Si, Ca, and Ti) have come to be known as α-elements, even though no single nuclear reaction produces their excesses.

Historically, the decline in [O/Fe] (and other α-elements) versus [Fe/H] from the MW halo to disk has been assumed to result from the time delay between Type II and Type Ia supernovae (hereafter SNe II and SNe Ia), first detailed by Tinsley (1979). In this scenario, oxygen is produced first by the short-lived SNe II, while iron is produced by both SNe II and SNe Ia; the SNe Ia contribution occurred on longer timescales than the SNe II. In this way, SNe Ia iron was added after a time delay for SNe Ia onset.

This SNe Ia time-delay chemical evolution scenario was explored and supported by the detailed calculations by Matteucci & Brocato (1990), which predicted that the decline to lower [O/Fe] in systems with low star formation rates (henceforth SFRs), like the LMC, should occur at lower [Fe/H] than in the MW disk. Similarly, the [O/Fe] decline should occur at higher [Fe/H] in high-SFR systems, like giant elliptical galaxies and bulges.

The average [α/Fe], derived from our measured O, Mg, Si, Ca, and Ti abundances, is −0.04 dex, −0.11 dex, and −0.03 dex for stars 242, 247, and 266, respectively (see Table 7). The average [α/Fe], at −0.06 dex, is close to the solar value, consistent with the scaled-solar model atmospheres employed for the abundance analysis. However, it is notable that the most [Fe/H]-rich star, 247, has the lowest [α/Fe] ratio, at −0.11 dex.

Figure 2 shows a comparison of the average Sgr [α/Fe] ratios found here with other works. The [α/Fe] ratios measured by SM02 and C10 agree remarkably well. Results for stars 242 and 266 here are consistent with these papers, although on the lower envelope; however, [α/Fe] for star 247 (the most Fe-rich star) is lower by ∼0.1 dex. We note that the spatial location of the stars studied here and those in SM02 and C10 possess considerable overlap, with roughly the same mean position within Sgr.

The S07 [O/Fe] and [Si/Fe] trends are similar to that found by C10. On the other hand, S07 found sub-solar [α/Fe] values for their sample of 12 Sgr stars, lower than other studies by 0.1–0.3 dex, with the difference increasing to higher [Fe/H]. This deficiency in S07 is dominated by unusually low [Ti/Fe]

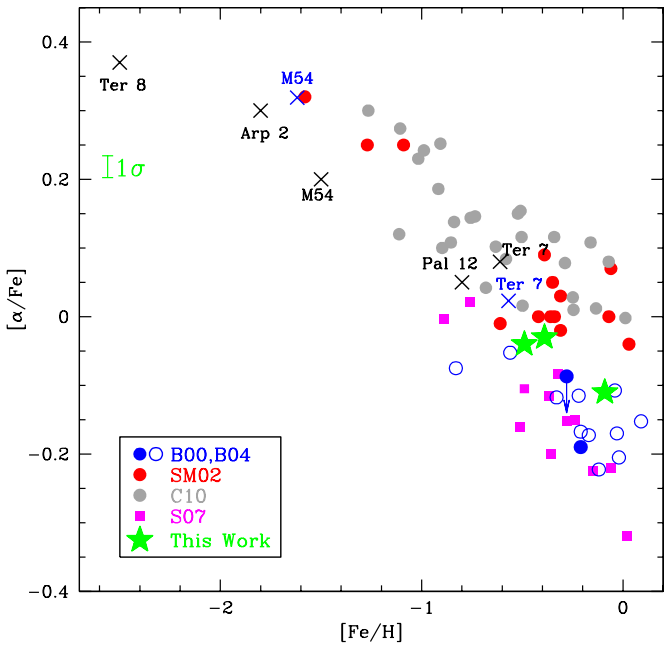

Figure 2. [α/Fe] ratios in Sgr. Crosses indicate globular clusters associated with Sgr: Terzan 8 and Arp 2 (Mottini et al. 2008), M54 (Brown et al. 1999; Carretta et al. 2010), Pal 12 (Cohen 2004), and Ter 7 (Sbordone et al. 2007). Sgr field stars are indicated for previous works: filled gray circles (Carretta et al. 2010; C10), filled red circles (Smecker-Hane & McWilliam 2002; SM02), filled and open blue circles (Bonifacio et al. 2000, 2004; B00; B04), and filled magenta squares (Sbordone et al. 2007; S07). The Sgr field stars studied in this work are represented by filled green stars.

(A color version of this figure is available in the online journal.)

and quite low [Ca/Fe] and [Mg/Fe] abundance ratios; these sub-solar [Ca/Fe] ratios are not seen in the MW disk at any metallicity. Only star 247 from our sample has sub-solar [Ca/Fe]. Therefore, there is either a systematic error in the S07 [α/Fe] values or a different composition for the S07 Sgr field, which is located 22 arcmin west of the stars in this work, SM02, and C10. Clearly, further investigation of the low α-element abundances found by S07 is warranted.

We note that a long-known disparity between Ti I and Ti II abundances may have contributed to the low [Ti/Fe] ratios in S07 and other papers. The cause of the Ti ionization imbalance has recently been shown to be due to non-LTE effects on Ti I by Bergemann (2011). Bergemann (2011) finds that Ti I non-LTE corrections of +0.25 dex are required for the very metal-poor RGB star HD 122563 ([Fe/H] = −2.5); whether the correction would be similar for solar-metallicity RGB stars is not known. Although substantial absolute non-LTE abundance corrections for Ti I are indicated, the line-by-line differential LTE abundance analysis of bulge and disk giants by Fulbright et al. (2007) found Ti ionization imbalance of only ∼0.05 dex. Presumably, the non-LTE effect in the Fulbright program stars was canceled out by use of Arcturus as a differential standard. Our results show excellent agreement between Ti I and Ti II measurements, with a mean ε(Ti I)−ε(Ti II) abundance difference of 0.00 dex and an rms scatter of 0.10 dex. Thus, by employing a differential line-by-line analysis, we believe that we have minimized systematic problems with non-LTE corrections to the Ti I abundances.

Our [α/Fe] ratios are slightly higher than, but on the upper envelope of, the results of B00 and B04; notably, B04 did not measure Ti abundances for their stars. Thus, our [α/Fe] points lie close to the average of C10/SM02 and S07/B00/B04. The

[α/Fe] values for the Sgr fields near M54, studied here and by SM02 and C10, are lower than the solar neighborhood thin-disk trend by ∼0.18 dex.

The [O/Fe] ratio in our three stars is ∼0.3 dex below the trend in the solar neighborhood measured by Allende Prieto et al. (2004); however, our [O/Fe] ratios are only 0.18 dex below the solar neighborhood disk trend found by Edvardsson et al. (1993). The difference between these two comparisons is that in the latter the Sun is at the upper end of the distribution of [O/Fe] ratios at [Fe/H] = 0.0, while in the former study the Sun has an unusually low [O/Fe] for its metallicity. Thus, the difference lies in the systematic effects present in Edvardsson et al. (1993) and Allende Prieto et al. (2004). Unsurprisingly, our measured [O/Fe] ratios are consistent with McWilliam & Smecker-Hane (2005a, henceforth MS05), which are deficient relative to the solar neighborhood by 0.17 dex. The [O/Fe] deficiencies in C10 are slightly lower, by as much as 0.10 dex, than the results found in this work. The S07 [O/Fe] results are also ∼0.1 dex lower than found here, similar to their generally low [α/Fe] ratios. In the SNe Ia time-delay paradigm of Tinsley and Matteucci & Brocato the low [O/Fe] ratios indicate a lower SFR in Sgr than the solar neighborhood.

4.3. Lithium

Our Li abundances, based on the λ6707 line, are +0.42, +0.14, and −0.47 dex for stars 242, 247, and 266, respectively. Although the EWs of the Li I line in stars 242 and 247 are quite large, at 137 and 103 mÅ, this is due to the cool stellar temperatures rather than high Li abundances.

Because of their similar age ranges and metallicities, it is sensible to compare the Li abundances of our Sgr stars with Li abundances for red giant stars in the Galactic disk. A comparison of our Li abundances with the LTE abundance survey of solar neighborhood GK giants by Brown et al. (1989) shows that our stars fall near the peak of the Li-abundance frequency distribution function and thus appear quite normal. We calculate that our three stars fit the distribution of Li abundances in Brown et al. (1989) with $\chi^2 = 1.10$. We note that the mean and standard deviation of the Li detections in Brown et al. (1989) are 0.48 and 0.69 dex, respectively, while the mean and standard deviation of our three stars are 0.03 and 0.46 dex, respectively. Clearly, it will be necessary to measure Li abundances in a larger sample of Sgr stars before systematic differences between Sgr and the MW disk can be detected. For now, it appears that whatever causes a range of Li abundance in solar neighborhood giants also applies to the Sgr RGB stars.

Extensive non-LTE calculations for Li have been performed (e.g., Carlsson et al. 1994) that suggest Li abundance corrections to the LTE values near +0.25 dex for our stars, so the maximum non-LTE Li abundance for our stars is +0.6 dex. However, we note that the Brown et al. (1989) sample has considerable overlap with our stars in [Fe/H] and $T_{\rm eff}$. Thus, any non-LTE corrections to the Li abundances for our Sgr stars are likely to be similar to those for local RGB stars in Brown et al. (1989). Again, our stars show the normal range of Li abundances found for GK giants in the Galactic thin disk.

4.4. Sodium and Aluminum

In Figure 3 we compare the [Na/Fe] ratios found here with the Galactic disk studies of Reddy et al. (2003) and Bensby et al. (2005) and with the Sgr work of SM02, S07, and B00. We find excellent agreement with these previous Sgr works.

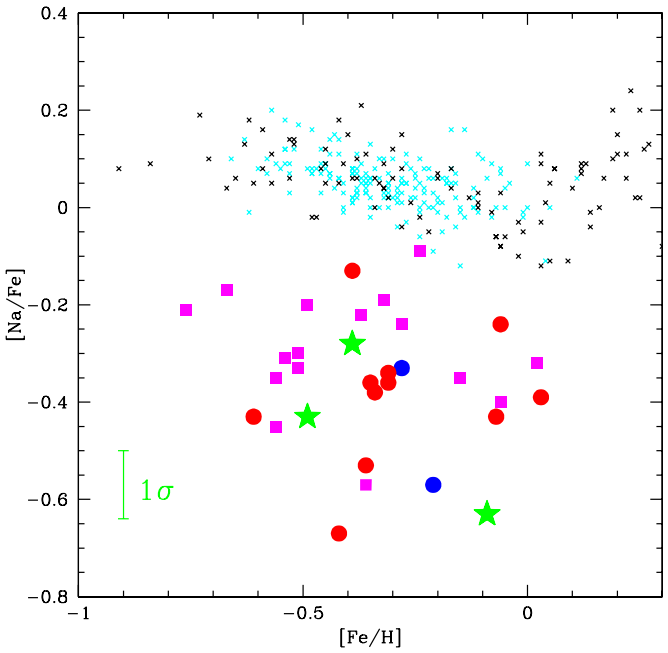

Figure 3. [Na/Fe] for our program stars (filled green stars) compared to the Galactic thin-disk measurements of Bensby et al. (2005; black crosses) and Reddy et al. (2003; cyan crosses). Sgr results from SM02 are represented by filled red circles, filled blue circles indicate B00, and filled magenta squares represent S07. Our program stars show the ∼0.4 dex [Na/Fe] deficiencies seen in Sgr by SM02, S07, and Bonifacio et al. (2000); such deficiencies are seen in other dwarf galaxies by various authors.

(A color version of this figure is available in the online journal.)

In all four investigations the Sgr stars are deficient relative to the solar neighborhood stars, and all, except S07, are consistent with ∼0.4 dex deficiencies (S07 found an average deficiency of ∼0.3 dex). We note that 0.3–0.4 dex deficiencies in [Na/Fe] are commonly seen in abundance studies of other dwarf spheroidal galaxies (e.g., Shetrone et al. 2001, 2003).

Figure 4 is similar to Figure 3, but also includes the C10 Sgr and M54 data points and a larger scale. A striking feature in Figure 4 is the high [Na/Fe] ratios for the most metal-rich Sgr stars in the C10 sample; this is inconsistent with all other Sgr studies to date. We believe that these high C10 [Na/Fe] ratios are probably erroneous, perhaps resulting from blended and saturated Na I lines measured with relatively low resolution spectra. In our spectra the λλ5682 and 5688 lines, used by C10, are too strong and blended to give reliable results; consequently, in this work we derived Na abundances from the neutral lines at 6154 and 6161 Å.

We note that C10 applied the non-LTE corrections of Gratton et al. (1999) to their abundances. Gratton et al. (1999) suggest typical Na non-LTE abundance corrections at +0.10 to +0.17 dex (for [Fe/H] = −0.5 and −0.1); this falls far short of the ∼0.5 dex upward shift required to bring SM02, B00, and our results close to the C10 values. Thus, C10's non-LTE corrections cannot explain their relatively high [Na/Fe] ratios, as seen in Figure 4. Calculations by Lind et al. (2011) found non-LTE corrections for Na I lines in cool giants near 0.1–0.2 dex, similar to Gratton et al. (1999). However, Lind et al. (2011) did not confirm the trend to large non-LTE corrections, up to +0.5 dex, for the lowest gravity stars claimed by Gratton et al. (1999). A check on the non-LTE abundance effect on Na in cool red giant stars comes from a comparison of LTE [Na/Fe] ratios for K giants and FGK dwarf stars in the Galactic disk, performed

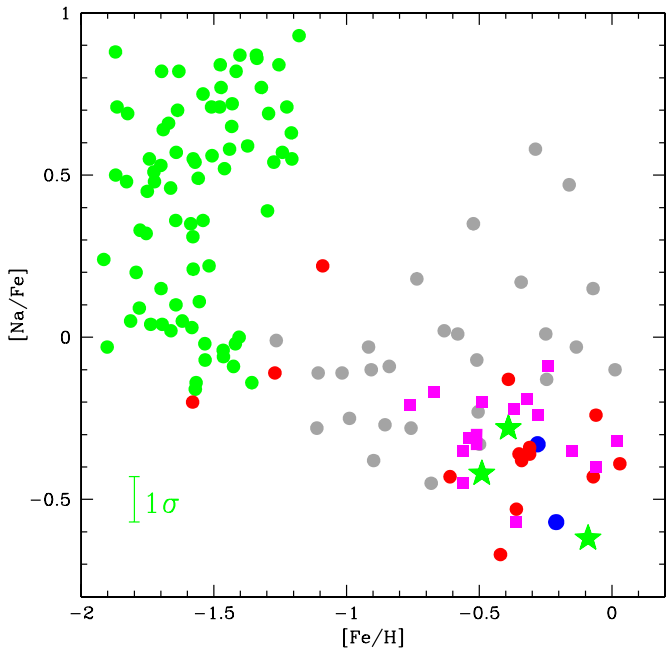

Figure 4. Larger scale plot of [Na/Fe] vs. [Fe/H] for Sgr/M54. Filled green stars indicate our program stars. Also shown are results from C10 for M54 (green filled circles) and Sgr dSph (gray filled circles). Red filled circles are from SM02; magenta squares show S07 points; blue circles are from B00. Note that [Na/Fe] ratios in Sgr found by S07 and B00 agree with this work, while C10 [Na/Fe] ratios are higher by ∼0.5 dex for [Fe/H] > −0.5 dex.

(A color version of this figure is available in the online journal.)

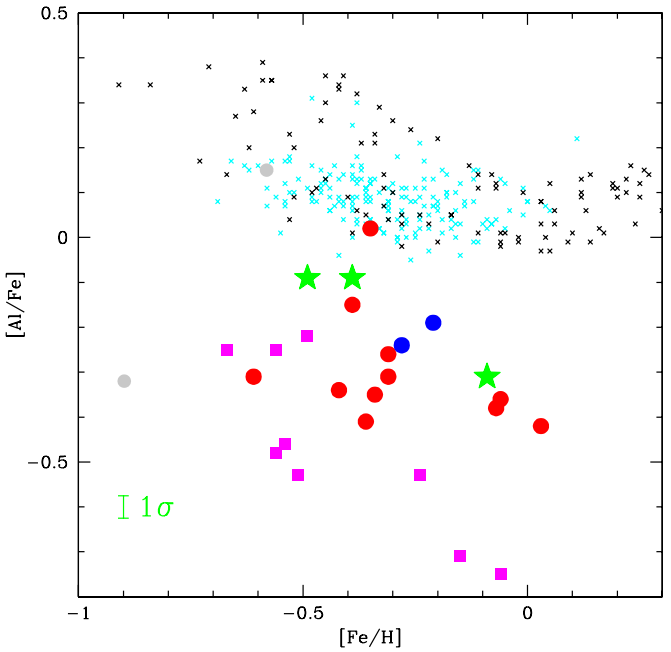

Figure 5. [Al/Fe] for our program stars (filled green stars) compared to the Galactic thin-disk measurements of Bensby et al. (2005; black crosses) and Reddy et al. (2003; cyan crosses). Sgr values from other studies are the same as in Figure 2. Of our stars, only 247 shares the ∼0.3 dex deficiency found by SM02 for Sgr, while stars 242 and 266 lie between the MW disk and other reported Sgr [Al/Fe] ratios. S07 give the lowest [Al/Fe] values. Generally, the S07 [X/Fe] ratios appear lower than the SM02 and C10 studies of Sgr.

(A color version of this figure is available in the online journal.)

by Fulbright et al. (2007). The excellent agreement between the dwarf and RGB star [Na/Fe] versus [Fe/H] trends indicated that non-LTE effects must be similar and likely small.

The main nucleosynthesis source of sodium is thought to be carbon burning, after core carbon ignition in massive stars that ultimately end as SNe II (e.g., Woosley & Weaver 1995). However, roughly 10% of the ^{23}Na is produced by hot-bottom proton burning of hydrogen-rich envelope material by the Ne-Na cycle (Woosley & Weaver 1995).

McWilliam & Smecker-Hane (2005a) and SM02 pointed out that the Na and Al deficiencies are consistent with a paucity of material ejected from core-collapse SNe and/or a low SNe II/SNe Ia ratio, similar to the argument for the low [α/Fe] ratios in dwarf galaxies.

The extensive detailed abundance study of M54 by C10 found oxygen deficiencies and sodium enhancements for a large fraction of the cluster stars. This Na–O anti-correlation is seen in most Galactic globular clusters (e.g., Carretta et al. 2009) and is evidence that the cluster was polluted by proton-burning products during its formation. As shown by C10, M54 stars exhibit a tight correlation in the [Na/Fe] versus [O/Fe] plane, presumably due to dilution of the proton-burning products with unprocessed material. We note that our three stars, as well as those of S07, lie far from the locus of points in C10's plot of [Na/Fe] versus [O/Fe] for M54, consistent with the idea that our stars are members of Sgr, rather than M54, showing no detectable signature of pollution by proton-burning products.

In Figure 5 we compare [Al/Fe] measured here with results from previous studies of Sgr and the Galactic thin disk; symbols are the same as in Figures 2–4. The median [Al/Fe] across all studies shown in Figure 5 is near −0.3 dex. However, results for stars 242 and 266 in this work are slightly higher, both at −0.09 dex. Our star 247, at [Al/Fe] = −0.31, is similar to that of SM02, but about 0.2 dex higher than the [Al/Fe] ratios found by S07. Carretta et al. (2010) measured [Al/Fe] for only two Sgr stars, at +0.15 and −0.32. In general, our [Al/Fe] ratios confirm the Al deficiencies found in all other studies of Sgr; however, it remains to be determined whether the small differences between studies are real. Similar, low-[Al/Fe] ratios have also been identified in the Sculptor dwarf galaxy by Geisler et al. (2005). Al abundances have not often been measured for stars in other Local Group dwarf galaxies, perhaps because the lines were not detected.

As with other low-ionization neutral species, it seems possible that non-LTE effects might significantly affect the computed LTE Al abundances. Some non-LTE studies for Al lines have been performed (e.g., Gehren et al. 2006; Andrievsky et al. 2008); however, these have focused on metal-poor stars, much more metal-poor than our Sgr stars, and/or stars whose temperatures are ∼2000 K hotter than the cool red giants studied here. An eyeball extrapolation of the Andrievsky et al. (2008) non-LTE corrections to the temperatures and [Fe/H] values of our stars suggests corrections ∼0.2–0.3 dex, with a considerable uncertainty. The Gehren et al. (2006) non-LTE calculations suggest corrections of ∼0.1–0.3 dex for our stars, although no extrapolation in gravity parameter is possible.

As with Na, Fulbright et al. (2007) compared LTE [Al/Fe] versus [Fe/H] trends from RGB and dwarf stars in the Galactic disk. They found a systematic offset, such that the RGB star [Al/Fe] ratios needed to be reduced by 0.08 dex in order to come into agreement with the dwarfs. This 0.08 dex offset likely reflects the difference in non-LTE correction between the dwarfs and giants. This suggests that our RGB [Al/Fe] ratios probably need to be revised down by 0.08 dex, in order to compare to the Galactic disk dwarf trend. This would serve to increase

the apparent Al deficiency in Sgr, with the non-LTE corrected [Al/Fe] near −0.4 dex.

The [Al/Mg] ratios of our Sgr stars show no sign of the anti-correlation seen in globular cluster stars affected by proton-burning products. Similarly, our [Al/Mg] ratios differ significantly from the locus of globular cluster stars in M54, whose composition does exhibit signs of proton burning in the study of C10. Thus, there appears to be no evidence of proton-burning products in the atmospheres of our Sgr stars, based on both the [Al/Mg] and [Na/O] ratios.

Calculations by Woosley & Weaver (1995) showed that most Al is produced in hydrostatic carbon and neon burning; thus, like Na, Al is produced mostly by massive stars that end as SNe II. However, some Al is produced in the envelopes of intermediate-mass AGB stars by proton burning in the Mg–Al cycle (e.g., Karakas & Lattanzio 2003). Since Sgr stars show no evidence of contamination by such proton-burning products, we conclude that the observed Al deficiencies result from a paucity of SNe II material in this galaxy compared to the MW disk.

4.5. Iron-peak Elements

In addition to iron we have also measured LTE abundances for the iron-peak elements V, Mn, and Cu. All of these elements have odd numbers of protons and consequently possess strong hfs, which affects line formation through de-saturation. Abundances were computed using the measured EWs and the hfs line lists shown in Table 4.

4.5.1. Vanadium

The average [V/Fe] of our three stars is -0.02 ± 0.07 dex, completely consistent with the solar value. This is at odds with the results from S07, who found general vanadium deficiencies in Sgr, with an average [V/Fe] $= -0.40 \pm 0.05$ dex. However, from 14 Sgr stars Smecker-Hane & McWilliam (unpublished) found the average [V/Fe] $= 0.00$ with 1σ scatter of 0.13 dex, in good agreement with this work. C10 did not measure vanadium abundances. We suspect that the S07 V deficiencies are spurious, possibly due to adopted low $T_{\rm eff}$ values. Low temperatures may also account for the lower [α/Fe] values found by S07 than other studies. However, the S07 results may indicate that V is more deficient farther from the Sgr nucleus.

On the other hand, expectations from chemical evolution models and SN nucleosynthesis (e.g., Timmes et al. 1995; Woosley & Weaver 1995; Arnett 1971) predict sub-solar [V/Fe] ratios at low [Fe/H], which has not yet been found in MW stars.

4.5.2. Manganese

The study of the [Mn/Fe] trend in Sgr, the MW disk, and the Sun is filled with contradictory conclusions; regrettably, our results add to this confusion. The one thing everyone agrees upon is that [Mn/Fe] increases from approximately −0.4 dex at [Fe/H] typical of the MW halo to +0.1 to +0.2 dex for disk stars with super-solar [Fe/H]. The Mn deficiency in metal-poor MW halo stars was first noted by Wallerstein (1962).

In Figure 6 we compare our [Mn/Fe] ratios with the MW disk and halo results from Feltzing et al. (2007, black crosses) and Sobeck et al. (2006, black open squares), respectively. Our three Sgr stars agree with the trend of these MW results.

It is notable that the S07 and McWilliam et al. (2003) [Mn/Fe] trends for Sgr lie ∼0.2 dex below the MW trend, and thus lower than the results for the three stars in this paper;

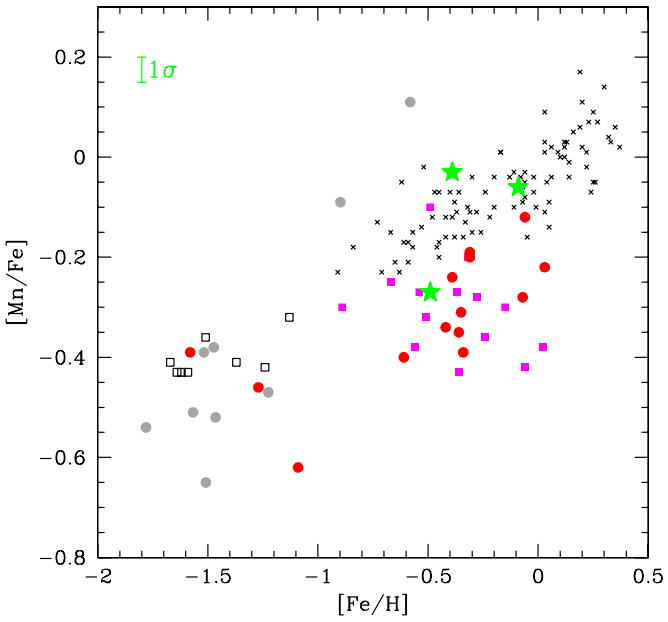

Figure 6. [Mn/Fe] for our program stars (filled green stars) compared to Sgr results from SM02 (filled red circles) and S07 (magenta squares). Two Sgr stars and seven M54 stars from C10 are indicated by gray filled circles. Also shown are solar neighborhood points from Feltzing et al. (2007; crosses) and Sobeck et al. (2006; black open squares). Our new results appear to be in better agreement with the MW trend, rather than previous Mn measurements for Sgr.
(A color version of this figure is available in the online journal.)

however, star 242 in this study is reasonably consistent with the previous studies of Mn in Sgr. Carretta et al. (2010) measured [Mn/Fe] for only two Sgr stars, but their values lie well above the trend in the MW disk and much higher than all other Sgr studies. Carretta et al. (2010) also measured [Mn/Fe] for seven stars in M54 and found values ∼0.1 dex lower than the Galactic globular cluster values of Sobeck et al. (2006). If we take this to indicate that a +0.1 dex correction is required for the C10 [Mn/Fe] values, this would increase the discrepancy between their two Sgr stars and all other studies. At the very least, it seems that the [Mn/Fe] values for the two Sgr stars in C10 are so anomalous that they are suspect.

While the [Mn/Fe] results for Sgr stars in this work are higher than other studies, we are wary about preferring one result over another. An analysis of Mn in the Sun, by Bergemann & Gehren (2007), showed that while non-LTE corrections to the solar Mn abundance were of order 0.05 dex, the laboratory oscillator strengths for the transitions show larger than expected discrepancies between studies, of order 0.1 dex. Bergemann & Gehren (2007) also derive systematically low Mn abundances for Mn I lines arising from levels with excitation potentials of 2–3 eV, similar to problems found for solar Fe I lines (e.g., Blackwell et al. 1982). In addition, there are long-standing differences between solar photospheric abundances from Mn I lines and the meteoritic value, sometimes by as much as 0.3 dex. Bergemann & Gehren (2007) confirm this lacuna and conclude that non-LTE and log gf value problems alone cannot account for such deviations, and they suggest that 3D hydrodynamical calculations may be required to understand the discrepancies. These problems suggest that the most robust way to estimate [Mn/Fe] values is with line-by-line differential abundance analysis, which is the method we have employed in this work. It is clear that further study is required in order to determine

whether the trend of [Mn/Fe] versus [Fe/H] is lower in Sgr than in the MW disk.

The [Mn/Fe] differences may be due to the absolute abundance technique employed by SM02 and McWilliam et al. (2003) and the paucity of photometric and reddening information available at the time, which made it difficult to constrain the atmosphere parameters of their stars. In contrast, for the current work we had access to extensive optical and infrared photometric data, and we have employed our line-by-line differential abundance method, relative to Arcturus, which we believe is superior to the method used by SM02. Furthermore, the [Mn/Fe] uncertainties of the absolute method were increased by the discrepancy between published solar photospheric and meteoritic values. While we believe that the techniques employed in this work are superior to SM02 and McWilliam et al. (2003), it is still possible that the [Mn/Fe] discrepancy could be due to the relatively low S/N of the current spectra.

If the final conclusion reached is that the [Mn/Fe] ratios in Sgr are deficient relative to the MW disk trend, then the conclusion of McWilliam et al. (2003) and Cescutti et al. (2008) holds: that metal-poor SNe Ia contributed a significant portion of the iron-peak material to the more metal-rich Sgr stars. This could have occurred during leaky-box chemical evolution, expected of dwarf galaxies.

Recently, Cunha et al. (2010) have found Mn deficiencies in stars belonging to the large Galactic globular cluster ω Cen, the only other place where [Mn/Fe] deficiencies relative to the MW trend have been claimed.

4.5.3. Copper

Figure 7 shows the [Cu/Fe] trend with [Fe/H] for our three stars compared to other Sgr studies, as well as M54 from C10 and MW stars from Mishenina et al. (2002) and Simmerer et al. (2003). Inspection of Figure 7 shows that our results share the Cu deficiencies seen in all studies of Sgr. However, our results are most similar to that of McWilliam & Smecker-Hane (2005b), with ∼0.5 dex [Cu/Fe] deficiency compared to MW stars; this agreement is not surprising given that the Cu hfs list was the same in the two studies. Although C10 only measured [Cu/Fe] for two Sgr stars, the results are in good agreement with this work and McWilliam & Smecker-Hane (2005b). On the other hand, S07 found [Cu/Fe] deficiencies that increased with increasing [Fe/H], such that by solar iron abundance the [Cu/Fe] ratio is near −1 dex. Whether this difference is real needs to be further investigated. If the extra Cu deficiencies in S07 are real, it would suggest chemical inhomogeneity, or a Cu gradient, in Sgr, since the S07 field is relatively distant from other Sgr studies considered here. One unexpected observation is that the C10 [Cu/Fe] ratios for M54 stars show a large range, roughly 0.6 dex; this might simply reflect large measurement uncertainties due to the relatively low resolution spectra employed by C10.

Similar [Cu/Fe] deficiencies to those found for Sgr have been measured in the massive Galactic globular cluster ω Cen by Cunha et al. (2002) and Pancino et al. (2002); notably, ω Cen also shows Mn deficiencies, similar to Sgr. Pompéia et al. (2008) found [Cu/Fe] deficiencies even for the highest [Fe/H] stars in the LMC; this adds to the chemical similarities of the LMC and Sgr, which includes sodium and α-element deficiencies and s-process enhancements. Nissen & Schuster (2011) have also found a sub-population of MW halo stars showing deficient Cu abundances, in addition to low [α/Fe], [Na/Fe], and [Al/Fe] ratios and high [Ba/Y] values; again, these abundance ratios are similar to those of Sgr. We agree with the conclusion of

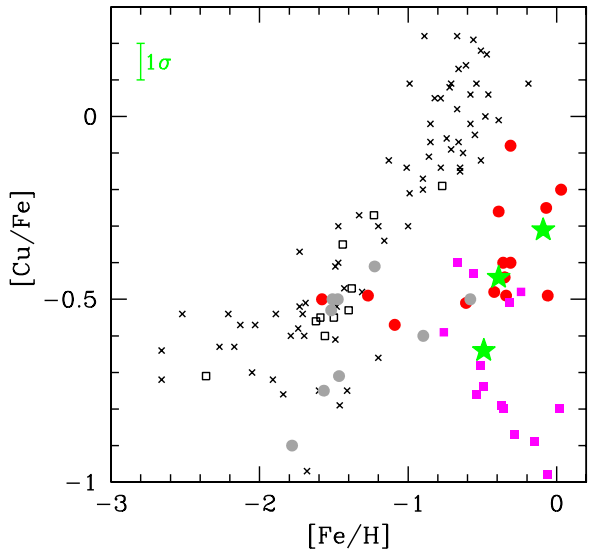

Figure 7. [Cu/Fe] for our program stars. Symbols are the same as in Figure 2. Also shown are solar neighborhood points from Simmerer et al. (2003; black open squares) and Mishenina et al. (2002; crosses). Clearly, Cu is deficient in Sgr compared to MW stars.

(A color version of this figure is available in the online journal.)

Nissen & Schuster (2011), that this sub-population reflects the accretion of late-time dwarf galaxies into the Galaxy.

Copper is thought to be predominantly produced in the hydrostatic He- and C-burning phases of massive stars (which ultimately become SNe II) via weak s-process neutron capture, driven by ^{22}Ne(α,n)^{25}Mg. This idea has been developed from calculations of the s-process in massive stars, including papers by Prantzos et al. (1990), Raiteri et al. (1993), The et al. (2000), Bisterzo et al. (2004), Chieffi & Limongi (2006), Pignatari et al. (2010), and Pumo et al. (2010, 2012). These papers indicate that the yield of copper increases with increasing metallicity, as expected from the metallicity dependence of the s-process, but also with the mass of the massive star, presumably due to the size of the He- and C-burning regions. However, significant complications arise in computing the Cu yields, due to such effects as nuclear reaction rates, convective overshoot, mass loss, and fallback; a number of the aforementioned papers discuss these difficulties. In addition, a minor component of the Cu is thought to be produced during explosive nucleosynthesis (e.g., Woosley & Weaver 1995).

In Figure 8 we show that the trends of [Cu/O] versus [Fe/H] in the MW thick disk and Sgr closely follow each other; this work supports the idea that Cu is mainly produced by massive stars that end as core-collapse SNe. However, the SM02 and S07 [Cu/O] ratios lie slightly below the thick-disk trend.

These conclusions about Cu production suggest that environments with a paucity of ejecta from massive stars should show Cu deficiencies. Given that massive stars are thought to be the major source of α-elements and Na and Al, the deficient Cu abundances should be accompanied by low α, Na, and Al abundances. These abundance patterns are, indeed, found in this work and in other studies of Sgr. Thus, the low [Cu/Fe] ratios suggest a low SNe II/SNe Ia ratio. Low SNe II/SNe Ia ratios may follow some time after a burst of star formation, due to the time delay between SNe II and SNe Ia, or can occur as a result of an initial mass function (IMF) deficient in high-mass stars (either top-light or from a steep IMF slope).

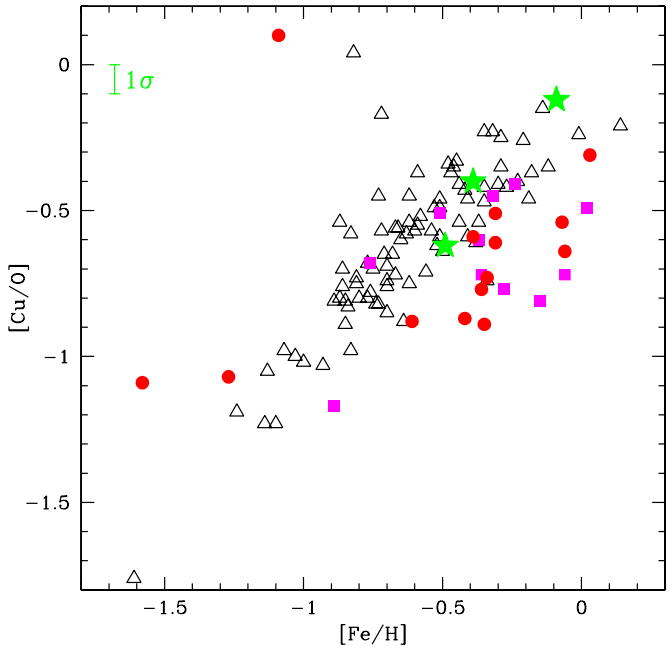

Figure 8. [Cu/O] vs. [Fe/H] for our program stars and other Sgr studies (symbols the same as in Figure 2) compared to the thick-disk results of Reddy et al. (2006; open black triangles). The similar metallicity-dependent [Cu/O] trend for the thick disk and Sgr is consistent with the idea that Cu is produced by the progenitors of Type II SNe, in agreement with Bisterzo et al. (2004) and many others. However, S07 and SM02 results show [Cu/O] ratios lower by ∼0.2 dex, although they also show an increasing trend with [Fe/H].

(A color version of this figure is available in the online journal.)

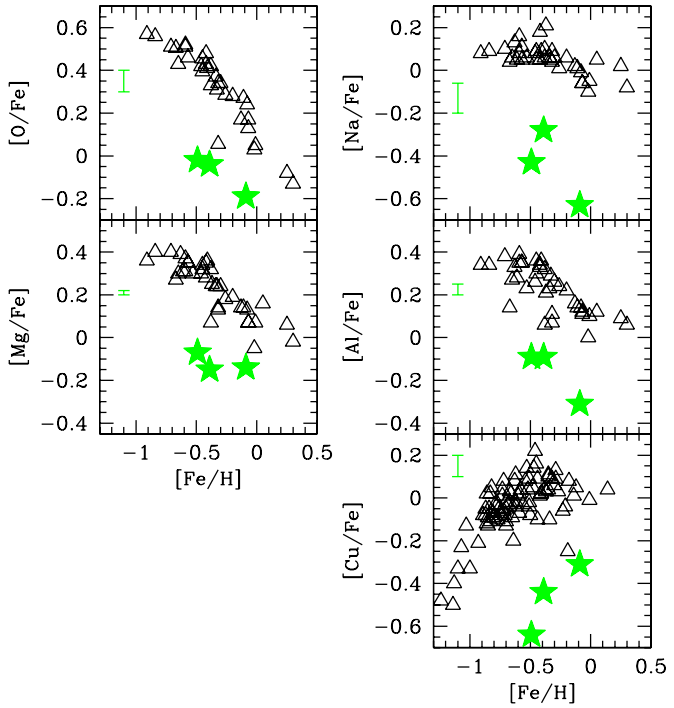

Figure 9. Comparison of the hydrostatic α-elements, O and Mg, Na, Al, and Cu in Sgr (filled green stars) with the thick-disk results of Bensby et al. (2005; open black triangles). The figures show that elements produced in the hydrostatic burning phases of SNe II progenitors are deficient, relative to iron, in all cases by more than a factor of two.

(A color version of this figure is available in the online journal.)

4.6. Hydrostatic and Explosive Elements

At this point we have mentioned a number of elements whose synthesis in massive stars is dominated by either hydrostatic helium-, carbon-, or neon-burning phases (e.g., O, Mg, Na, Al, and Cu), or in the SNe II explosion event (Si, Ca, Ti, and Fe). The yield of the hydrostatic elements increases with stellar mass; for Al, Na, and Cu the yields are also thought to be metallicity dependent (e.g., Arnett 1971; Prantzos et al. 1990; Woosley & Weaver 1995), despite the observed flat trend of [Na/Fe] in the Galactic disk.

The explosive elements are thought to be produced in both SNe II and SNe Ia events, with lower [X/Fe] ratios from SNe Ia than for SNe II events. However, the exact SNe Ia [Si/Fe], [Ca/Fe], and [Ti/Fe] yield ratios are not known, but lie somewhere below the solar value. Production of the hydrostatic elements by SNe Ia is thought to occur, but with negligibly small [X/Fe] ratios (e.g., Nomoto et al. 1984; Maeda et al. 2010). In this section we compare the abundances of the hydrostatic and explosive element families in Sgr with the MW thick disk.

To understand how Sgr evolved, we wish to compare our measured element abundance ratios to some standard population. We choose the MW thick disk as our standard reference because the thick-disk mean [Fe/H], near −0.6 dex, and [Fe/H] range, approximately from −2.0 to 0.0 dex are very similar to those of Sgr, because the thick-disk stellar ages cover a range of ∼5 Gyr (Reddy et al. 2006), similar to the age difference between the two Sgr populations studied by Siegel et al. (2007), and because the thick-disk composition is well measured. Thus, the metallicities and timescales are similar for these two systems, so chemical composition differences are less likely to be due to metallicity or timescale-dependent parameters.

Table 8
Sgr Thick-disk Element Differences

Species	Δ[X/Fe] (dex)
[O I]	−0.43 ± 0.03
Na I	−0.50 ± 0.09
Mg I	−0.34 ± 0.05
Al I	−0.39 ± 0.04
Si I	−0.14 ± 0.06
Ca I	−0.16 ± 0.05
Ti I	−0.20 ± 0.07
Ti II	−0.21 ± 0.08
Cu I	−0.50 ± 0.11

In Figure 9 we compare our Sgr hydrostatic element ratio measurements for [O/Fe], [Mg/Fe], [Na/Fe], [Al/Fe], and [Cu/Fe] with the thick-disk results of Bensby et al. (2005). For the explosively produced α-elements, we compare our Sgr [Si/Fe], [Ca/Fe], [Ti I/Fe], and [Ti II/Fe] ratios to Bensby's thick-disk trends in Figure 10. A glance at Figures 9 and 10 shows that the Sgr hydrostatic element [X/Fe] ratios lie much further below the thick-disk trend than the ratios for the explosively produced elements.

In Table 8 we list the Δ[X/Fe] abundance shifts, which would move the observed Sgr [X/Fe] ratios to the thick-disk trends; thus, the shift indicates the change in X required to transform the thick-disk abundance ratios into the measured Sgr values.

Clearly, in Figures 9 and 10 the addition of some amount of extra Fe to the MW trends can be used to reproduce the measured Sgr [X/Fe] and [Fe/H] ratios for each element, X; however, the amount of Fe required is different for each element: 0.7 dex is required for O, 0.5 dex for Na, Al, and Mg, 0.2 dex for Ca and

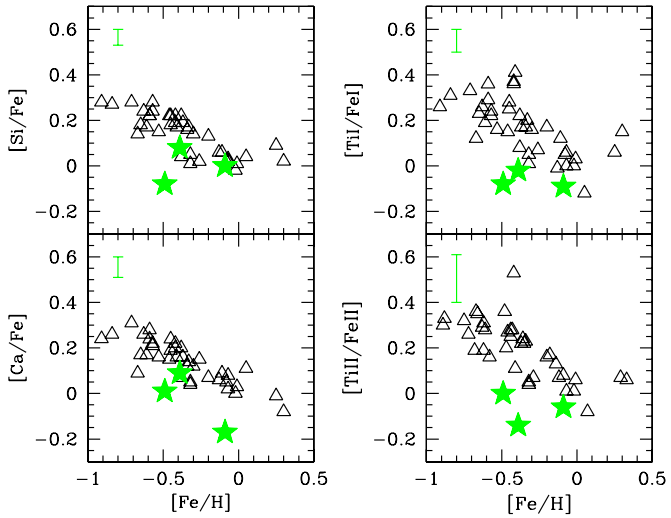

Figure 10. Comparison of the explosive α-elements, Si, Ca, and Ti, in Sgr (filled green stars) with the thick-disk results of Bensby et al. (2005; open black triangles). The figures show that explosive nucleosynthesis products of SNe II are deficient, relative to iron, by −0.17 dex, which is significantly less than the deficiency for the hydrostatic elements, at −0.43 dex.

(A color version of this figure is available in the online journal.)

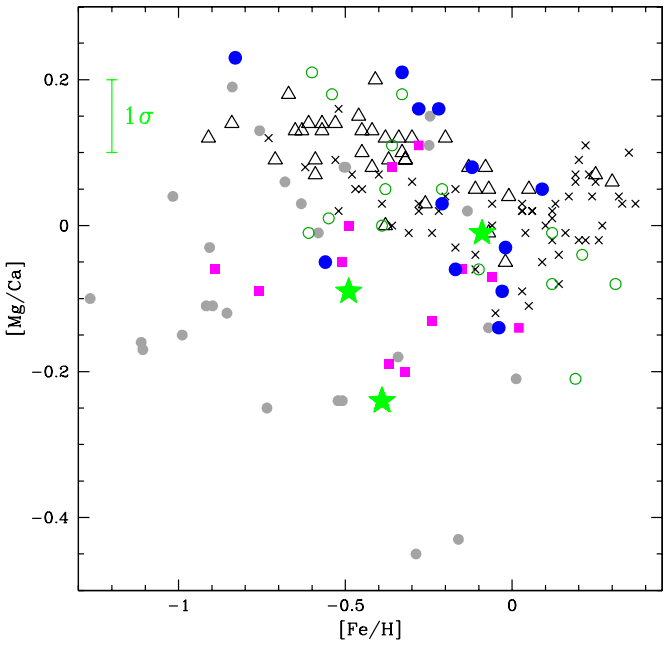

Figure 11. Trend of [Mg/Ca] vs. [Fe/H] in the thin disk (crosses; Bensby et al. 2005), thick disk (black open triangles; Bensby et al. 2005), and Sgr (symbols the same as Figure 2, except B00 and B04 are both represented by filled blue circles). The Sgr trend for C10 and S07 is ∼0.2 dex lower than the Galactic disk, while Sgr B00/B04 points are similar to the disk; our average [Mg/Ca] is lower than the MW disk by ∼0.1 dex. Both Sgr and the Galactic disk show a decline in [Mg/Ca] with increasing [Fe/H].

(A color version of this figure is available in the online journal.)

Si, 0.3 dex for Ti, 0.4 dex for Cu, and 0.0 dex for *r*-process Eu. Thus, it is not possible to reproduce the Sgr composition by adding a single quantity of Fe to the MW disk ratios, even for pure SNe II elements (such as O, Mg, Al, Na, and Cu); therefore, we do not consider this possibility further.

Table 8 demonstrates that the hydrostatic elements all possess rather large deficiencies, Δ[X/Fe], relative to the Galactic thick-disk trend. Within this group of hydrostatic elements, the individual Δ[X/Fe] values show a dispersion that may be real, for example, Δ[Mg/Fe] = −0.34 dex while Δ[Na/Fe] = −0.49 dex; however, the group is reasonably represented by the mean Δ[X/Fe] = −0.40 ± 0.04 dex. Similar α-element deficiencies have been found in previous abundance studies of dwarf galaxies (e.g., Shetrone et al. 2001, 2003; Geisler et al. 2005) as well as in sub-populations of the Galactic halo (e.g., Brown et al. 1997; Nissen & Schuster 1997; also see Venn et al. 2004).

In Table 8 the explosive elements show smaller deficiencies for [Si/Fe], [Ca/Fe], and [Ti/Fe], relative to the thick disk, at −0.14, −0.16, and −0.21 dex, respectively, with a mean Δ[X/Fe] = −0.17 ± 0.03 dex. Thus, the explosive element [X/Fe] ratios, relative to the thick disk, are 0.25 dex higher than for the hydrostatic elements.

The unusually low abundance ratio of hydrostatic to explosive elements is also seen in the [Mg/Ca] ratios from previous Sgr studies, as shown in Figure 11. The Sgr results of C10 and S07 are, on average, deficient in [Mg/Ca], relative to the MW disks, by −0.19 dex, in agreement with our result. However, the [Mg/Ca] ratios given by B00 and B04 are similar to the MW disk trend. These details notwithstanding, all studies show a steady decline in [Mg/Ca] with increasing [Fe/H], by 0.4 dex/dex for Sgr and 0.2 dex/dex for the MW disk.

The Δ[X/Fe] differences between hydrostatic and explosive elements suggest a relative paucity of nucleosynthesis products from the most massive SNe II events, a conclusion that is bolstered by our inclusion of Na, Al, and Cu as hydrostatic elements. These deficient hydrostatic/explosive abundance ratios can be explained by at least two scenarios: enrichment by an IMF deficient in the most massive SNe II progenitors, or from nucleosynthesis with excess SNe Ia, perhaps due to long-lived SNe Ia progenitors that contribute metals over an extended period.

Support for both mechanisms can be found in the literature: Weidner & Kroupa (2005) and Kroupa et al. (2011) predicted a steeper integrated galactic IMF (IGIMF) for dwarf galaxies (like Sgr). They argued that, with less total gas mass than the MW, dwarf galaxies lack the most massive molecular clouds and so are less efficient at producing the most massive stars. Kroupa et al. (2011) also predicted an IGIMF slope that steepened with increasing metallicity. Likewise, Oey (2011) showed that the IMF slope steepens when there is insufficient gas to make the largest molecular clouds. Our Sgr low hydrostatic/explosive abundance ratios, including [Mg/Ca], suggest an IMF deficient in the most massive stars, because the yield of hydrostatic elements increases with increasing SNe II progenitor mass.

On the other hand, the SNe Ia time-delay scenario of Tinsley (1979) has long been invoked to explain the decline in [O/Fe], and other α-elements, with [Fe/H] in the MW disks. Indeed, Matteucci & Brocato (1990) predicted deficient [O/Fe] ratios in the LMC due to its presumed low SFR compared to the MW. Our low hydrostatic/explosive element ratios might also be understood in this scenario, since SNe Ia produce Si, Ca, and Ti but not O, Na, Mg, Al, and Cu in significant quantities. A particular difficulty is that Fe and the explosive αs can be produced both by low-mass SNe II and by SNe Ia, so without good constraints on the element yields it is not easy to disentangle the relative role of these two nucleosynthesis sources. Thus, the decline of [Mg/Ca] in the MW disks and Sgr could be explained by a metallicity-dependent IMF over the range from [Fe/H] = −1 to 0, or by an increasing

nucleosynthetic contribution of Ca from SNe Ia events over the formation times of the disk and Sgr.

Tolstoy et al. (2003) claimed that the low [α/Fe] ratios seen in dwarf galaxies were evidence of steep IMFs, with reduced contributions from massive stars; however, their argument was specious as it omitted other scenarios. In a subsequent paper the same group (Venn et al. 2004) asserted that low [α/Fe] ratios could occur without affecting the IMF, by the addition of material from SNe Ia.

We note that our [O/Mg] ratios in Sgr, correlated with O/hydrostatic ratios, lie precisely on the declining [O/Mg] trend with [Mg/H] for the MW bulge and disks, noted by McWilliam et al. (2008). The decline in [O/Mg] is thought to be due to a quenching of oxygen yields from massive stars as metallicity-dependent winds strip their outer layers (McWilliam & Rich 2004; McWilliam et al. 2008; Cescutti et al. 2009). From [Fe/H] $= -1$ to the solar value, at least $\sim$0.2 dex of the decline in [O/Fe] must be due to metallicity-dependent stellar wind effects.

4.7. The s-process Elements

In this work we employ La II lines to indicate abundances for elements in the second *s*-process peak. The La II lines are strong enough for reliable EW measurement, and the hyperfine constants are well measured. Thanks to a large nuclear spin, $I = 7/2$, the hfs is so significant that the La II lines remain on the linear part of the curve of growth to quite large EWs; this greatly enhances the accuracy of our abundance measurements. However, we are not able to measure reliable barium abundances, because even the weakest Ba II line, at 5853 Å, is too strongly saturated (EW $>$ 200 mÅ), even for the most metal-poor star in our sample. This is a consequence of the large *s*-process enhancements in Sgr.

Figure 12 shows [La/Fe] versus [Fe/H] found here, compared to the Sgr results of SM02, S07, B00, and the solar neighborhood Galactic stars of Simmerer et al. (2004). Our [La/Fe] ratios agree well with all previous studies of Sgr, showing enhancements of $\sim$0.5 dex. This chemical signature further strengthens the conclusion that these stars are, indeed, members of Sgr. Clearly, the stars of Sgr are significantly enhanced in La compared to the solar neighborhood, which suggests *s*-process enrichment. This is seen in stars of several other nearby dwarf spheroidal galaxies (e.g., Shetrone et al. 2001, 2003; Pompéia et al. 2008; Geisler et al. 2005; Letarte et al. 2010). It is interesting that S07 and SM02 both find a single Sgr star with [La/Fe] $\sim$ 1 dex, near solar metallicity, significantly higher than the trend of [La/Fe] with [Fe/H]. It is not clear whether this is due to a narrow spike in [La/Fe] or reflects inhomogeneity. At this point we should note that a study of Sgr M giants, by Chou et al. (2010), found sub-solar [La/Fe] ratios, near -0.2 dex, more than $\sim$0.5 dex lower than the [La/Fe] ratios found here and by SM02 and S07; the Chou et al. (2010) results also showed a peak-to-peak scatter of $\sim$1 dex near solar [Fe/H]. Given the difficulty of measuring [La/Fe] in M giants, the scatter, and the discordant nature of the Chou et al. (2010) results, we choose not to use them for further comparison.

We note that in Figure 12 the solar neighborhood points of Simmerer et al. (2004) show a small decline in [La/Fe] above [Fe/H] ~ -0.4 dex. We believe that this trend is real and results from the metallicity-dependent decline in the production of the heavy *s*-process elements (e.g., Gallino et al. 1998; Busso et al. 1999).

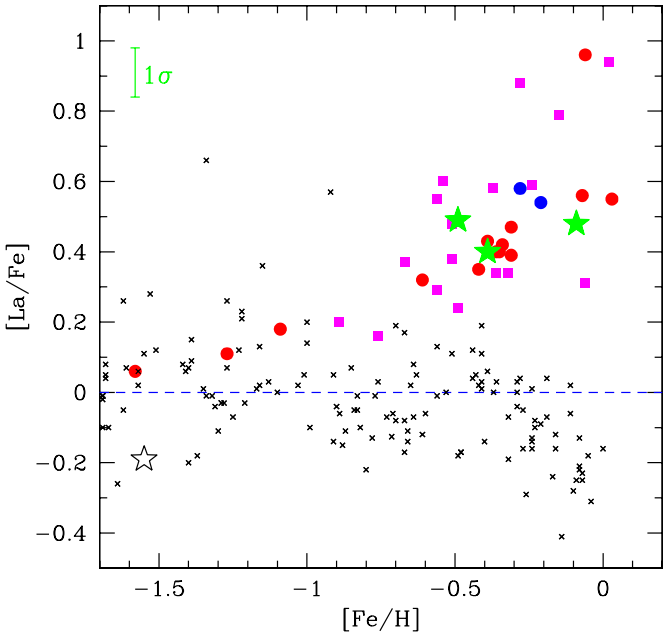

Figure 12. [La/Fe] in Sgr stars (see Figure 2 for symbol key). Also shown are solar neighborhood points from Simmerer et al. (2004; crosses) and M54 from Brown & Wallerstein (1999; black open star).

(A color version of this figure is available in the online journal.)

Following MS05, in Figure 13 we compare [La/Eu] versus [La/H] for our three stars with SM02 and B00. The [La/Eu] ratio distinguishes between *r*-process and *s*-process neutron capture. The [La/H] abscissa in the plot, as employed by MS05, allows metallicity discrimination without the complication of [Fe/H]. Both La and Eu are made by neutron-capture processes, but Fe is made by explosive nucleosynthesis processes by SNe Ia and SNe II. Thus, plotting [La/Eu] with [La/H] avoids the added complexity and uncertainties, due to the production of Fe, in addition to neutron-capture processes. The loci in Figure 13 are dilution curves showing the evolution of the composition with the addition of pure *s*-process material for the solid line, and 95% *s*-process with 5% *r*-process for the dashed line. We note that the three points from this work follow a slope roughly consistent with the addition of pure *s*-process to an earlier composition, although offset by $\sim$0.1 dex higher than the values found by SM02 and MS05. Whether these abundance differences are real, due to inhomogeneities in Sgr, or resulted from the different measurement techniques is not yet certain; however, the agreement is within the measurement uncertainties. The similarity of [La/Eu] versus [La/H] in this work with SM02 and B00 supports our assertion that our stars are, indeed, members of Sgr. As discussed by MS05, the slope of the locus in Figure 13 shows enrichment by essentially pure *s*-process material, with no significant *r*-process production above [La/H] ~ -0.4 to -0.6 dex (corresponding to [Fe/H] ~ -0.6 to -0.8 dex, respectively). However, the *r*-process [Eu/H]$_r$ ratios increase with [Fe/H] among our small sample, showing that some *r*-process enrichment occurred during the evolution of Sgr, but at a much lower level than the *s*-process.

4.7.1. Heavy and Light s-process

As discussed by Gallino et al. (1998) and Busso et al. (1999), the ratio of heavy to light neutron-capture elements, [hs/ls], produced by the *s*-process, is sensitive to metallicity. For the *s*-process in low-mass AGB stars the neutrons are

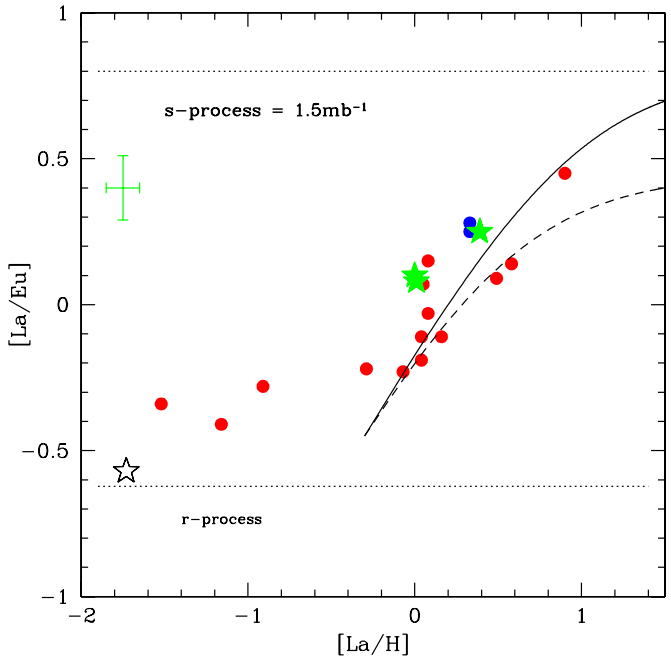

Figure 13. [La/Eu] for our program stars (filled green stars) compared to Sgr following SM02 (filled red circles), two points from B00 (filled blue circles), and M54 by Brown et al. (1999; open black star). The horizontal dotted lines show pure *s*-process and *r*-process [La/Eu] ratios. The solid line shows a dilution locus, resulting from the addition of pure *s*-process material, while the dashed line shows the dilution locus for 95% *s*-process plus 5% *r*-process added to an *r*-process-dominated starting composition.

(A color version of this figure is available in the online journal.)

predominantly produced via the $^{13}C(\alpha,n)^{16}O$ reaction, where the ^{13}C results from $^{12}C(p,\gamma)^{13}N(\beta+\nu_e)^{13}C$ following ingestion of protons from the envelope. In low-metallicity AGB stars, a roughly constant number of neutrons released in the thermal pulse are captured by very few iron-peak nuclei, and most of the seed nuclei end up as heavy *s*-process elements (e.g., Ba, La, Pb). However, at higher metallicity the numerous seed nuclei, on average, capture many fewer neutrons and so produce more of the light *s*-process elements (e.g., Sr, Y, Zr) than the heavy *s*-process elements.

Figure 14 shows [La/Y] versus [Fe/H] for our stars, compared to MS05,[4] S07, and B00. The [La/Y] ratios for our stars share the range of [hs/ls] enhancements seen in nearby dwarf spheroidal galaxies, such as the 0.5–0.8 dex range found by Shetrone et al. (2001, 2003); see also Letarte et al. (2010), B00, and SM02. The [La/Y] enhancements for our Sgr stars indicate *s*-process nucleosynthesis by relatively metal-poor AGB stars [Fe/H] ~ -0.6 or $\leqslant -1$ dex (Busso et al. 1999), but the exact value depends on details of the predicted [hs/ls] curve. The [Fe/H] values indicated by the measured [La/Y] ratios are lower than the [Fe/H] of the stars themselves, particularly the more metal-rich Sgr stars; thus, neither the stars nor any companion could have produced the observed *s*-process enrichments. This indicates that the nearly ubiquitous *s*-process enhancements seen in Sgr are primordial and must have come from previous generations that enriched the interstellar gas, out of which the current stars formed. This novel way to produce *s*-process-rich stars (or barium stars), suggested by SM02, can result from leaky-box chemical evolution, where at late times

[4] MS05 revised the Y abundances measured by SM02 using gf values from Hannaford et al. (1982).

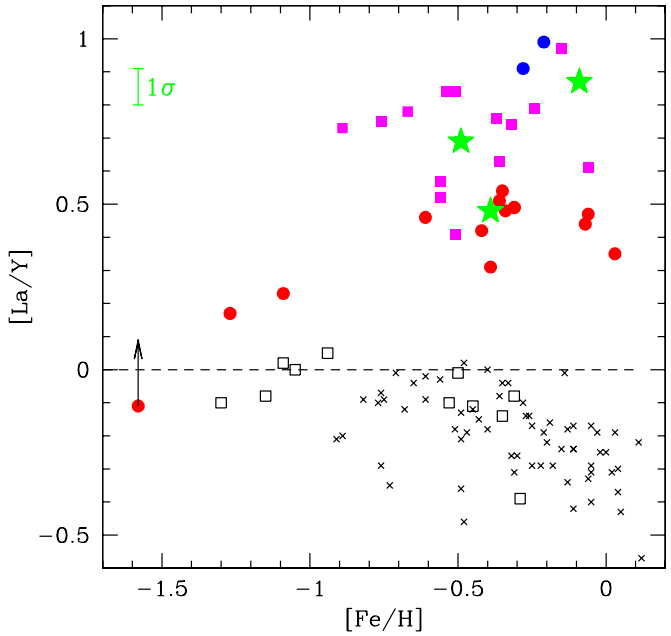

Figure 14. [La/Y] for Sgr stars (see Figure 2 for key) and solar neighborhood stars indicated with black crosses (Simmerer et al. 2004) and black open squares (Gratton & Sneden 1994).

(A color version of this figure is available in the online journal.)

gas from a large, old, metal-poor population can dominate the composition of the younger population of metal-rich stars.

Here we confirm that [La/Y] enhancements are present in Sgr, as found by B00, SM02/MS05, and S07; our values overlap most with S07 and B00, whereas the SM02/MS05 values are lower than the current results.

Due to limited wavelength coverage, SM02/MS05 had access to three to four less than optimal Y II lines, including the line at 7450 Å, with a poorly known gf value. In the present work we have measured [Y/Fe] using six Y II lines for Arcturus and five lines in the Sgr stars. Unlike SM02/MS05, the differential technique used here is unaffected by poorly known gf values; however, our spectra have lower S/N than SM02/MS05 and we have only one star with [Fe/H] $\geqslant -0.1$ dex, while SM02/MS05 had three such stars. The current results, particularly for star 247, combined with the two points of B00 and the S07 results, indicate an increasing trend of [La/Y] with increasing [Fe/H], from [La/Y] $\sim$ 0.0 dex at [Fe/H] ~ -0.7 to [La/Y] $\sim +1$ dex by solar [Fe/H]. Such an increase is also seen in the [La/Y] and [Ba/Y] ratios in Fornax, measured by Letarte et al. (2010). Because high [La/Y] values are characteristic of nucleosynthesis in low-metallicity AGB stars (Gallino et al. 1998; Busso et al. 1999), it appears that the most metal-rich Sgr stars formed out of material dominated by ejecta from metal-poor AGB stars. Our highest [La/Y] value (for star 247) is reproduced by the detailed calculations of Bisterzo et al. (2010), but is higher than the predictions of Cristallo et al. (2009, 2011) by ~0.25 dex. A small increase in the amount of protons ingested into the intershell region is required, above the standard treatment (ST), for the Cristallo et al. (2009, 2011) calculations to reproduce the observed [La/Y] ratio of star 247.

Figure 15 shows [La/Y] versus [La/H] for the stars studied in this work, compared to Sgr stars studied by MS05/SM02, S07, and B00. For each source we show the measured abundance ratios with filled symbols and the *r*-process-subtracted ratios with open symbols. The *r*-process corrections were computed using [Eu/Fe] and [La/Fe] ratios and adopting *r*-process ratios

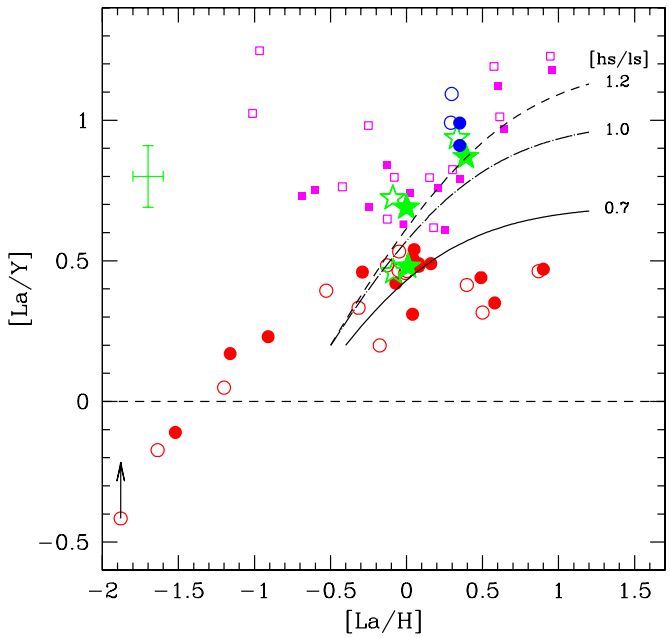

Figure 15. [La/Y] vs. [La/H] for our Sgr stars (green stars) compared to Sgr results of SM02 (red circles), B00 (blue circles), and S07 (magenta squares). Filled symbols show the measured abundance ratios; open symbols indicate *r*-process-subtracted values. The solid black line is a dilution curve showing the effect of adding the highest predicted [La/Y] AGB *s*-process yields ([La/Y] = +0.70 dex) of Cristallo et al. (2011) to the pre-existing Sgr composition, near [La/H] = −0.40 dex ([Fe/H] = −0.70). The dot-dashed line shows a dilution curve resulting from the addition of [La/Y] = +1.00 dex material to Sgr gas at [La/H] = −0.50 ([Fe/H] = −0.76), [La/Y] = +0.20, and the short-dashed locus indicates dilution with [La/Y] = +1.2 material. Except for the SM02 results, the measurements suggest that the *s*-process in Sgr produced much higher [La/Y] ratios than the AGB predictions of Cristallo et al. (2011).

(A color version of this figure is available in the online journal.)

for $[\mathrm{La/Eu}]_r = -0.58$ dex and $[\mathrm{La/Y}]_r = +0.57$ dex. These *r*-process ratios were based on the solar *s*- and *r*-process fractions determined by Bisterzo et al. (2011), Simmerer et al. (2004), and Arlandini et al. (1999) and the abundance ratios in the *r*-process-rich star CS 22892–052 (Sneden et al. 1996).

We used the measured [Eu/Fe] ratios for the *r*-process corrections to apply to the heavy-element abundances in MS05/SM02, B00, and this work, but for S07 no Eu abundances were measured. Consequently, for the S07 points we employed [Fe/H] and the observed thick-disk [Eu/Fe] versus [Fe/H] trend to estimate [Eu/Fe]. That is a reasonable assumption, given the good agreement with the thick-disk trend for *r*-process [Eu/Fe] ratios measured here and in B00 (see Figure 17).

Figure 15 shows that the *r*-process corrections are typically less than 0.1 dex for stars above [La/H] ∼ −0.2 dex and therefore do not significantly affect our conclusions.

It is immediately obvious that the MS05/SM02 results, above [La/H] ∼ +0.3, lie significantly below the values from the three other Sgr studies, suggesting that MS05/SM02 [La/Y] ratios may be in error. This might reasonably have resulted from the use of blended Y II lines in the SM02 list, or the use of Y II lines with poorly known gf values in the absolute analysis of SM02. Such difficulties not withstanding, all Sgr studies show significantly enhanced [La/Y] compared to the MW disk.

The solid line in Figure 15 represents a dilution curve, starting with the pre-existing composition at [La/H] = −0.40 and [La/Y] = +0.20 dex, and adding pure metal-poor AGB *s*-process ejecta based on the theoretical [La/Y] yields from Cristallo et al. (2011). In this case we employ the predictions from their $z = 1.0 \times 10^{-3}$, $1.5\,M_{\odot}$ model, which happens to give their maximum expected [La/Y] value. Unfortunately, this locus severely underpredicts the [La/Y] ratios compared to the majority of Sgr studies, including the present work. If the MS05/SM02 [La/Y] values are disregarded, then the AGB *s*-process [La/Y] yields must be higher than the Cristallo et al. (2011) predictions. The dot-dashed line in Figure 15 shows the dilution locus assuming an intrinsic *s*-process [La/Y] ratio of +1.00 dex and starting at [La/H] = −0.5 dex (corresponding to [Fe/H] = −0.76), while the short-dashed line is the locus for dilution with [La/Y] = +1.2 dex.

These high [La/Y] dilution loci provide a superior comparison to the measured abundance ratios; however, they are 0.3 and 0.5 dex higher than the maximum predicted AGB *s*-process [La/Y] yields. As noted earlier, the [La/Y] = +1.0 dilution locus is in better agreement with the [Fe/H] = −1.0 AGB *s*-process predictions of Bisterzo et al. (2010), at [La/Y] = +0.9 dex. However, to obtain [La/Y] = +1.00 dex, consistent with our second dilution curve, would require an increase of the mass of the ^{13}C pocket introduced into the intershell region to twice the standard value, or ST*2 in the format of Bisterzo et al. (2010).

We note that the dilution loci in Figure 15 assume that there is no significant contribution of *s*-process material from stars more metal-rich than [Fe/H] ∼ −0.5 dex. If this assumption is incorrect, then higher [Fe/H] AGB material would have been incorporated into Sgr, with characteristically lower [La/Y]. In that case, to match the [La/Y] ratios measured in this work by S07 and B00 would require an even larger increase in the mass of the ^{13}C pocket. Thus, our dilution curves provide a minimum estimate of the [La/Y] yield ratio (and ^{13}C pocket) for AGB stars near [Fe/H] = −0.6 dex.

The reasonable fit of the measured [La/Y] ratios to the [La/Y] = +1.2 dilution curve suggests that AGB stars with [Fe/H] > −0.5 dex did not dominate neutron-capture element nucleosynthesis in Sgr. This might be expected following a burst of star formation near [Fe/H] −0.7 to −0.6 dex and a trickle of stars to higher [Fe/H], where the composition is dominated by AGB stars from the peak of the main burst of star formation. This would tend to increase the yield of the second, or heavy, *s*-process peak elements, like La, qualitatively consistent with the large La overabundances toward increasing [Fe/H] and the [La/Eu] versus [La/H] trend seen in Figure 13.

If the relatively low [La/Y] ratios of MS05/SM02 are taken at face value, then chemical enrichment from AGB stars with [Fe/H] > −0.5 dex could explain the [La/Y] ratios and the roughly constant [La/Y] value toward higher metallicities. However, at the present time the weight of the published abundances is discordant with the MS05/SM02 [La/Y] values.

We note that abundance measurements of stars in the LMC, by Pompéia et al. (2008) and Van der Swaelmen et al. (2012), also show large [La/Y] overabundances, up to +1.0 dex, but with the trend shifted to lower [La/H]. Our dilution calculations indicate that the Pompéia et al. (2008) trend of [La/Y] with [La/H] in the LMC is consistent with an AGB dilution curve with [hs/ls] ∼ +1.1 dex, which confirms our conclusion for a higher than predicted [hs/ls] in Sgr.

Given the relatively good agreement between the Cristallo et al. (2009, 2011) *s*-process predictions and the abundances of MW stars enhanced with AGB-processed material, it is possible that we have identified a real difference between the [La/Y] ratios in the MW and the Sgr and LMC dwarf galaxies. However,

we do note the existence of at least two MW stars with [La/Y] larger than the predictions, for example: the metal-poor CH stars HE 0024–2523 (Lucatello et al. 2003) and G24–25 (Liu et al. 2012), both with [La/Y] = +0.85 dex.

While Sgr is enhanced in *s*-process material that has been ejected at the end of the AGB phase, we note that comparisons of theoretical *s*-process predictions with measured heavy-element abundances in MW stars have relied on current AGB stars and on mass-transfer objects, neither of which could have reached the final AGB *s*-process yields. It seems possible that this may explain part of the discrepancy in [La/Y] for Sgr and the MW.

We note that the [La/Zr] ratios are also enhanced, and we provide the same conclusion that metal-poor AGB stars contributed significantly to the material of the metal-rich Sgr stars. However, the [La/Zr] for star 247 is somewhat lower than our other two stars, indicating a declining [La/Zr] with increasing [Fe/H]. On the other hand, the [La/Rb] ratio increases with increasing [Fe/H], similar to the [La/Y] trend. Thus, we have to admit that we do not fully understand the [hs/ls] trends as well as we would like; however, for Rb, Y, and Zr the [hs/ls] ratios are super-solar, indicating that the metal-rich Sgr stars formed out of material dominated by metal-poor AGB stars.

4.7.2. Rubidium

Rubidium is thought to be strongly overproduced by intermediate-mass AGB stars (roughly 4–8 $M_{\odot}$) that experience high neutron fluxes via the ^{22}Ne(α,n)^{25}Mg reaction.

The *s*-process Rb yield is very sensitive to the neutron density, due to an unstable controlling isotope, ^{85}Kr, which blocks the production of ^{87}Rb at low neutron density. For intermediate-mass AGB stars temperatures are relatively high and ^{22}Ne(α,n)^{25}Mg occurs more readily, thus increasing the neutron density. At these high neutron densities ^{87}Rb is produced, but due to its small neutron-capture cross section it is not readily destroyed, resulting in a large equilibrium Rb abundance. This is the reason that [Rb/Zr] yields have been assumed to increase with increasing AGB mass (e.g., see the yields predicted in Smith et al. 2000).

Observationally, large Rb overabundances (up to 2–5 dex) have been claimed for intermediate-mass AGB stars in the Galaxy and the LMC by García-Hernández et al. (2006) and García-Hernández (2011), respectively. Recent theoretical calculations by van Raai et al. (2012) and Karakas et al. (2012) produce Rb enhancements in intermediate-mass AGB stars near ∼1 dex, which is similar to the mean for Galactic Rb-rich stars. They also find larger Rb enhancements at lower metallicity, as observed, but the maximum predicted [Rb/Fe] ratio, thus far, is +1.44 dex, significantly smaller than the most extreme observations.

Observational work and theoretical predictions for lower mass (1.3–3 $M_{\odot}$) stars indicate that the *s*-process neutrons are provided by the ^{13}C(α,n)^{16}O reaction (e.g., Lambert et al. 1995). In this case the ^{13}C is produced via ^{12}C(p,γ)^{13}N(β + ν_e)^{13}C following the ingestion of protons from the envelope into the He-H intershell region (e.g., Gallino et al. 1998). Notable, recent calculations of the resultant *s*-process yields for these stars have been performed by Cristallo et al. (2009) and Bisterzo et al. (2010).

Recent theoretical *s*-process yields for low-mass AGB stars (e.g., Cristallo et al. 2009, 2011; see the FRUITY[5] database) show a decline in [Rb/Zr] with increasing mass for AGB stars with masses ranging from 1.3 to 2.0 $M_{\odot}$; however, above a mass of ∼2.0 $M_{\odot}$, the [Rb/Zr] yield increases rapidly. Thus, there is not a linear increase in [Rb/Zr] with AGB star mass, and any attempt to determine a mean AGB mass or IMF slope from measured [Rb/Zr] ratios is complicated.

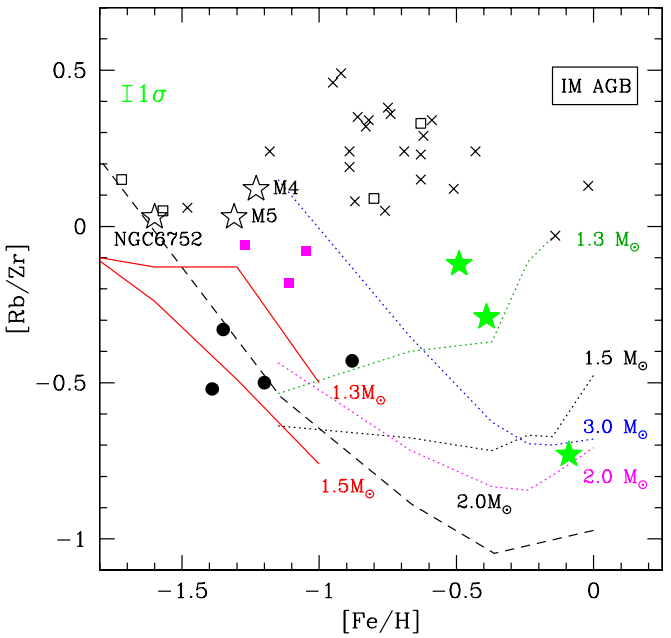

Figure 16. [Rb/Zr] for our program stars (filled green stars) compared to the Tomkin & Lambert (1999) solar neighborhood dwarfs and subgiants (black crosses) and giants (open black squares); CH stars in Tomkin & Lambert (1999) are indicated with filled magenta squares. Galactic globular clusters, M4, M5, and NGC 6752, measured by Yong et al. (2008, 2006) are marked with black open stars. Filled black circles indicate [Rb/Zr] ratios for ω Cen, based on Smith et al. (2000), which we have adjusted (see the text for details). Also shown are theoretical predictions for low-mass AGB stars, 1.3 and 1.5 $M_{\odot}$ by Bisterzo et al. (2010; red solid lines) and 2.0 $M_{\odot}$ from Cristallo et al. (2009; black dashed line). Dotted lines indicate the latest AGB *s*-process predictions from the FRUITY database. The theoretical prediction for intermediate-mass (5–7 $M_{\odot}$) AGB stars, computed by Karakas et al. (2012), is marked with a boxed "IM AGB."

(A color version of this figure is available in the online journal.)

Figure 16 shows a comparison of [Rb/Zr] for our three Sgr stars with the Galactic disk and halo. We have scaled the Smith et al. (2000) ω Cen [Rb/Zr] points to the solar meteoritic Rb/Zr ratio indicated by Lodders et al. (2009), at −0.19 dex. We have also adjusted the [Rb/Zr] ratios downward by 0.09 dex for the Tomkin & Lambert (1999) RGB stars, in order to account for their overestimated EWs of the solar Zr I lines at 6127.5 and 6143.2 Å. Our inspection of the profiles of these lines in the Kurucz solar spectrum reveals obvious blends, so our EW measurements are somewhat smaller than found by Tomkin & Lambert (1999); however, we do not see these blends in the Arcturus atlas of Hinkle et al. (2000). Although we should probably apply the same downward correction to the [Rb/Zr] ratios for both the dwarf and turnoff stars in Tomkin & Lambert (1999), we do not know whether their normalization relative to the Sun causes the effects of the blends to cancel out in the dwarfs; therefore, we have not applied the corrected Tomkin & Lambert (1999) Zr abundances for dwarf stars.

It is clear that the [Rb/Zr] ratios for our Sgr stars are well below the solar neighborhood, mostly thick-disk stars of Tomkin & Lambert (1999); our [Rb/Zr] ratios are also lower than the globular clusters, except for ω Cen, which has similar values. The Sgr [Rb/Zr] ratios decline roughly linearly with increasing

[5] FRUITY Web site http://fruity.oa-teramo.inaf.it/

[Fe/H], indicating the inclusion of progressively more material from low-mass AGB stars as metallicity increases. Thus, *s*-process nucleosynthesis in Sgr is driven by the $^{13}C(\alpha,n)^{16}O$ neutron source that operates in low-mass AGB stars.

The linear decline in [Rb/Zr] with increasing [Fe/H] suggests an initial [Rb/Zr] ~ 0.0 dex ratio, similar to the Galactic globular clusters, but near [Fe/H] $= -0.6$. This was followed by the addition of progressively more material from low-mass ($\sim 2\ M_{\odot}$) AGB stars as time and [Fe/H] increased. Certainly, there was no significant contribution to the [Rb/Zr] ratio in Sgr, above [Fe/H] $= -0.5$, by intermediate-mass AGB stars. If low-mass AGB material dominates in this way, then the most *s*-process-enhanced Sgr stars should show very low, or absent, ^{25}Mg and ^{26}Mg isotopes, as evidenced from their MgH line profiles.

Clearly, more points are required to verify the [Rb/Zr] versus [Fe/H] trend seen here. The similarity of the [Rb/Zr] values measured here for Sgr to the values in ω Cen, found by Smith et al. (2000), is yet another chemical signature shared between these two systems (e.g., McWilliam & Smecker-Hane 2005a, 2005b).

Lines in Figure 16 indicate predicted [Rb/Zr] yields for AGB stars as a function of metallicity and mass. The predictions show that intermediate-mass AGB stars (5–7 $M_{\odot}$) produce [Rb/Zr] $\sim +0.4$–0.5 dex (e.g., Karakas et al. 2012), while low-mass AGB stars yield much lower [Rb/Zr] ratios, as low as -1.0 dex. Also, there is a strong increase in [Rb/Zr] with decreasing [Fe/H] below metallicities corresponding to roughly [Fe/H] $= -0.5$ dex (e.g., Bisterzo et al. 2010; Cristallo et al. 2009).

These theoretical predictions indicate that the [Rb/Zr] ratio for our most metal-rich Sgr star, 247, is inconsistent with AGB *s*-process below [Fe/H] ~ -1.0. Since the metallicity of M54 is below this metallicity, at [Fe/H] ~ -1.6 dex (Brown et al. 1999; Carretta et al. 2010), it follows that the neutron-capture elements in star 247 cannot have been produced by a low-mass M54 AGB star. If dilution is responsible for the observed linear trend of [Rb/Zr] with [Fe/H] in our three Sgr stars, then M54 AGB stars could not have been responsible for their neutron-capture elements. On the other hand, it is possible that the [Rb/Zr] ratio in star 247 could have been produced by an AGB star near [Fe/H] ~ -0.6 dex, roughly the mean metallicity of Sgr.

The low [Rb/Zr] ratios in Figure 16 indicate that the ratio of intermediate-mass to low-mass AGB stars in Sgr must have been much lower than for the MW disk and halo. This enhanced enrichment from low-mass AGB stars is consistent with the large *s*-process enhancements already noted. It is possible that these relatively low [Rb/Zr] ratios could result from an IMF that is heavily weighted to the lowest mass stars (a bottom-heavy IMF); however, such a conclusion regarding the IMF is not yet warranted.

Following a burst of star formation, material from low-mass AGB stars can dominate the gas composition at later times if a significant amount of the gas is lost from the system after the burst, i.e., leaky-box chemical evolution. Such outflows were suggested by SM02 to explain the high [La/Y] ratios (characteristic of low-metallicity AGB stars) found even for the highest metallicity Sgr stars. An important point is that the [La/Y] ratios require the dominance of metal-poor AGB material from the burst of star formation (near [Fe/H] ~ -0.6 dex) to the late-time, higher metallicity gas. The Sgr metallicity distribution function (MDF; e.g., Bellazzini et al. 2008; C10) and the Sgr mean [Fe/H] being lower than the MW is qualitatively consistent with a loss of gas reducing the formation of higher metallicity stars.

Even a system that does not leak, but does not experience significant gas inflows, could be expected to show lower [Rb/Zr] ratios than the MW disk, which is characterized by continuous star formation and gas infall.

In one version of a leaky-box scenario, following a burst of star formation, at any time after the burst the chemical composition of the gas is dominated by the stars from the burst that are currently ejecting their envelopes. Thus, as time and metallicity increase, the gas composition, as well as the composition of the diminishing younger stellar populations, is dominated by the ejecta of progressively lower mass, older stars. The exact mix of older and younger material would depend, in part, on the rate of gas leakage from the galaxy and the amount of star formation following the main event.

Detailed chemical evolution models fit to the measured chemical abundance patterns will be required to determine whether a bottom-heavy IMF or leaky-box model better explains the low [Rb/Zr] ratios in Sgr; however, we favor the leaky-box scenario because outflows are more likely in low-mass galaxies, like Sgr, whose gravity is less able to retain hot or high-velocity SN ejecta.

Regarding timescales, from Figure 16 it is clear that the low [Rb/Zr] ratio for star 247 could have been produced by a 2 $M_{\odot}$ AGB star; the main-sequence lifetime of such stars is ~ 1 Gyr (e.g., Pietrinferni et al. 2004). Thus, there was plenty of time between the 4–6 Gyr and 2.3 Gyr star formation bursts in Sgr (Siegel et al. 2007) to reduce the [Rb/Zr] ratio with material from low-mass AGB stars. The 2 $M_{\odot}$ AGB stars might even have enriched Sgr with *s*-process elements *during* the burst of star formation 4–6 Gyr ago. Notably, the age gap between the 4–6 Gyr and 2.3 Gyr populations indicates sufficient time to permit the lowest mass *s*-process-producing AGB stars, at 1.3 $M_{\odot}$ (e.g., Busso et al. 2004), with main-sequence lifetimes of ~ 3 Gyr, to enrich the late-time gas in Sgr.

4.8. The r-process and [Eu/O]

In Figure 17 we show the observed [Eu/Fe] versus [Fe/H] for the three stars studied here, compared to results from B00 and SM02; the SM02 Eu abundances have been reduced downward by 0.08 dex to correct an arithmetic error in the original work. We also compare to the [Eu/Fe] ratios for the Galactic thin and thick disks from Bensby et al. (2005).

McWilliam & Smecker-Hane (2005a) found enhanced [Eu/Fe] ratios in Sgr, but concluded that these could reasonably be due to *s*-process contributions to the Eu abundances. While their argument was plausible, based on the very strong La and Ba lines that indicated strong *s*-process enhancements, they did not compute the Eu *s*- and *r*-process fractions in their Sgr stars. Here, we compute the Eu *r*-process fractions, $f(\mathrm{Eu})_r$, for our three stars, using the equation

$$f(\mathrm{Eu})_r = \frac{1 - R_*/R_s}{1 - R_r/R_s}, \tag{3}$$

where

$$R_* = \left(\frac{N(\mathrm{La})}{N(\mathrm{Eu})}\right)_* = 10^{\varepsilon(\mathrm{La})_* - \varepsilon(\mathrm{Eu})_*},$$

$$R_r = \left(\frac{N(\mathrm{La})}{N(\mathrm{Eu})}\right)_r = 10^{\varepsilon(\mathrm{La})_r - \varepsilon(\mathrm{Eu})_r},$$

$$R_s = \left(\frac{N(\mathrm{La})}{N(\mathrm{Eu})}\right)_s = 10^{\varepsilon(\mathrm{La})_s - \varepsilon(\mathrm{Eu})_s}.$$

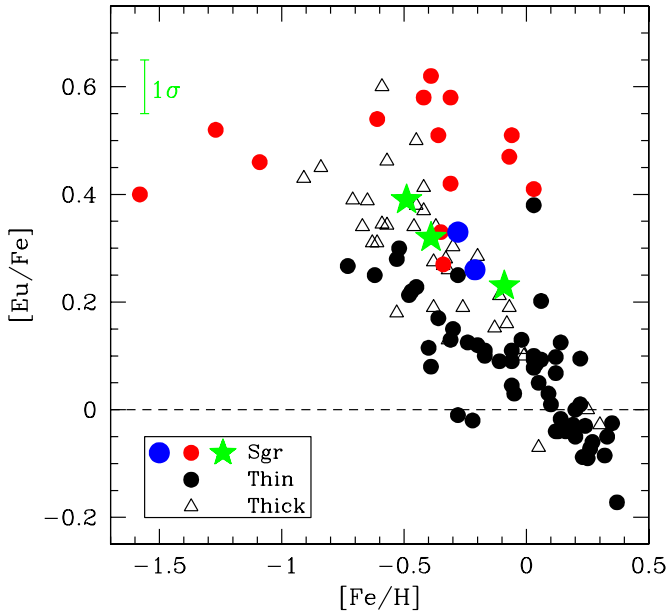

Figure 17. Plot showing the [Eu/Fe] ratio vs. [Fe/H] for stars in the Galactic thin and thick disk (black filled circles and open triangles, respectively) from Bensby et al. (2005) compared with measurements of Sgr stars: filled green stars (this work), filled red circles (SM02), and blue open circles (B00).

(A color version of this figure is available in the online journal.)

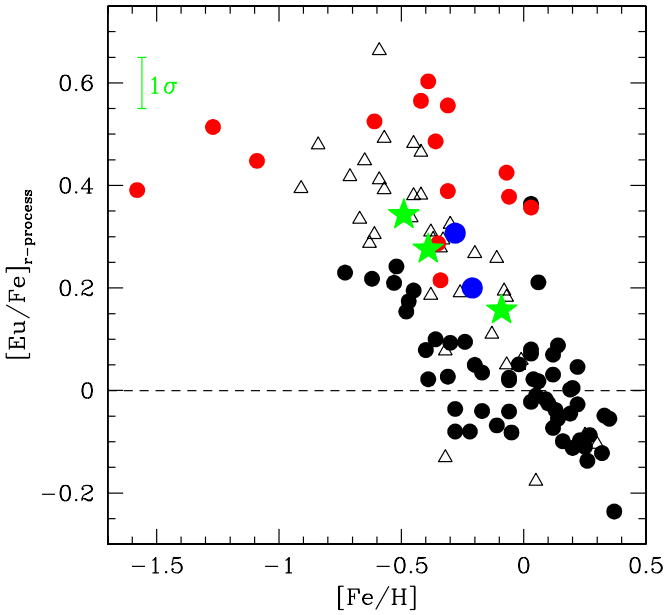

Figure 18. Plot showing the *r*-process $[Eu/Fe]_r$ ratio vs. [Fe/H] for stars in the Galactic thin and thick disk (black filled circles and open triangles, respectively) from Bensby et al. (2005) compared with Sgr: filled green stars (this work), filled red circles (SM02), and blue open circles (B00). See the text for a description of how the *s*-process fraction was subtracted in order to obtain the *r*-process, $[Eu/Fe]_r$, values.

(A color version of this figure is available in the online journal.)

Subscripts "*s*" and "*r*" refer to pure *s*-process and *r*-process values, respectively; the asterisk indicates values for the star under consideration.

Critical inputs to Equation (3) are the pure *r*- and *s*-process La/Eu number ratios. The *r*-process [La/Eu] ratio is taken from residuals to the solar system Nσ curve by Käppeler et al. (1989), Burris et al. (2000), and Simmerer et al. (2004), giving $[La/Eu]_r$ of −0.58 dex, on the Lodders et al. (2009) meteoritic scale (where $\epsilon(La/Eu)_\odot = +0.66$ dex); this is identical to the [La/Eu] abundance ratio, measured by Sneden et al. (1996), for the *r*-process-rich star CS 22892–052.

The *s*-process ratio is more difficult to assign, mainly because the exact [La/Eu] value depends on the details of the *s*-process site, including the stellar mass and metallicity. For example, a strong *s*-process computed by Malaney (1987) gave $[La/Eu]_s = +0.85$ dex for a single neutron exposure of $\tau = 1.5$ mb^{-1}; much more recently, Cristallo et al. (2009) predicted $[La/Eu]_s = +0.877$, $+1.076$, and $+0.95$ dex for $2\,M_\odot$ AGB stars with metallicities of 0.0, −0.36, and −0.66 dex, respectively; and other AGB predictions, by Arlandini et al. (1999) and Bisterzo et al. (2010), give similar *s*-process [La/Eu] values. Thus, it appears that there is general agreement on the theoretically predicted *s*-process ratios, near +0.88 dex; however, the *N*σ fits to the solar abundance distribution, by Burris et al. (2000) and Simmerer et al. (2004), gave significantly higher ratios, both indicating $[La/Eu]_s = +1.47$ dex.

Our computed Eu *r*-process fractions, $f(Eu)_r$, based on the lowest theoretical $[La/Eu]_s$ values, near $+0.88$ dex (Cristallo et al. 2009), are 0.86, 0.79, and 0.87 for stars 242, 247, and 266, respectively. If we adopt $[La/Eu]_s = +1.47$ from Simmerer et al. (2004) and Burris et al. (2000), we obtain $f(Eu)_r$ values of 0.97, 0.95, and 0.97, respectively. Thus, it is clear that despite the *s*-process enhancements in our Sgr stars, their Eu abundances are still dominated by the *r*-process. In the worst case the maximum correction to apply to the total Eu abundance, in order to obtain the *r*-process Eu abundance, is −0.10 dex.

In the following discussion we adopt a compromise value of $[La/Eu]_s = +1.00$ dex; for this case we find $f(Eu)_r$ of 0.90, 0.84, and 0.90 for stars 242, 247, and 266, respectively. We apply Equation (3) with the same $[La/Eu]_s$ to compute $f(Eu)_r$ for Eu abundances in SM02 and B00; we also add the −0.08 dex correction to Eu abundances in SM02 to correct an arithmetic error in their work. To compute *r*-process Eu abundances, we simply add $\log_{10} f(Eu)_r$ to the measured Eu abundances. The largest correction to SM02 Eu abundances is for their most metal-rich and La-rich star, at $[La/Fe] = +0.96$, with an $\varepsilon(Eu)$ correction of −0.13 dex. Typical *r*-process corrections for SM02 Eu abundances were a mere −0.02 dex. When these corrections were applied to this work and B00 for Sgr and to the Bensby et al. (2005) MW disk results, our $[Eu/Fe]_r$ values and those of B00 lie in excellent agreement with the MW thick-disk values, as seen in Figure 18; however, the SM02 results still lie above the MW $[Eu/Fe]_r$ trend with [Fe/H].

The similarity between the MW disk and Sgr *r*-process $[Eu/Fe]_r$ trend with [Fe/H] is particularly striking in comparison to the deficient trend of [O/Fe] with [Fe/H] in Sgr. It is not possible to explain both the decline of [O/Fe] and $[Eu/Fe]_r$ in Sgr with the late addition of iron from SNe Ia, as used by Tinsley (1979) to explain the [O/Fe] trend in the MW disk.

In Figures 19 and 20 we show the *r*-process $[Eu/O]_r$ and $[Eu/Mg]_r$ for Sgr stars in this work, SM02, and B00, compared with the MW thin- and thick-disk results of Bensby et al. (2005). Mg and O are thought to be produced mainly in the hydrostatic burning phases of massive stars that end as SNe II. The filled black circles and open black triangles in Figure 19 indicate the thin- and thick-disk stars, respectively. As noted by Bensby et al. (2005), the MW [Eu/O] ratio is flat, near the solar value, over more than 1 dex in [Fe/H], suggesting that Eu and O were formed in similar environments. This is consistent with the widely accepted idea that the *r*-process likely occurs in

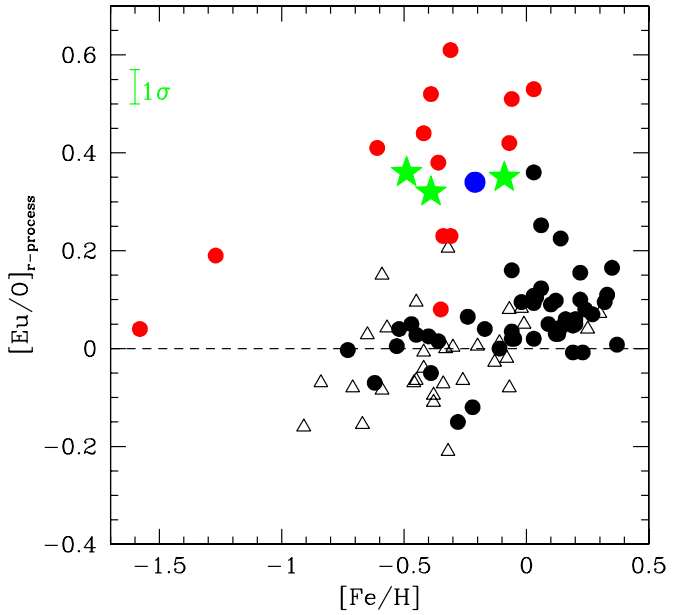

Figure 19. Plot showing the *r*-process $[Eu/O]_r$ ratio vs. [Fe/H] for stars in the Galactic thin and thick disk (black filled circles and open triangles, respectively) from Bensby et al. (2005) compared with Sgr stars: filled green stars (this work), filled red circles (SM02/MS05), and blue open circle (B00). The Sgr stars show an $[Eu/O]_r$ enhancement of ∼0.35–0.40 dex, while the disk ratio is relatively constant over 1.5 dex in [Fe/H]. Note that pure *s*-process [La/Eu] = +1.0 was assumed in the calculation of the europium *r*-process fraction, $f(Eu)_r$.

(A color version of this figure is available in the online journal.)

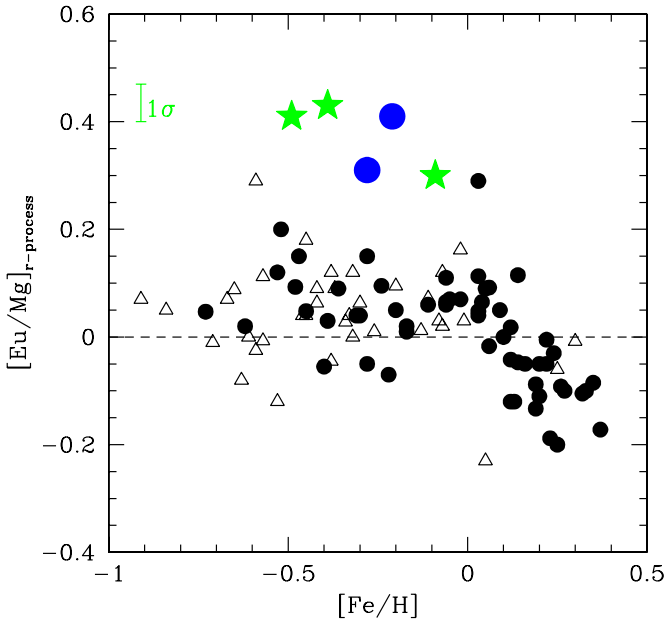

Figure 20. Plot showing the *r*-process $[Eu/Mg]_r$ ratio vs. [Fe/H] for stars in the Galactic thin and thick disk (black filled circles and open triangles, respectively) from Bensby et al. (2005) compared with Sgr: filled green stars (this work) and blue open circles (B00). Sgr shows an $[Eu/Mg]_r$ enhancement of ∼0.40 dex. Note that pure *s*-process [La/Eu] = +1.0 was assumed in the calculation of the europium *r*-process fraction, $f(Eu)_r$.

(A color version of this figure is available in the online journal.)

SNe II; certainly, the *r*-process timescale, of ∼1 s, suggests a sudden dramatic event, typical of SNe. However, theoretical investigations into the *r*-process have yet to identify a viable mechanism (e.g., see Nishimura et al. 2012). Figures 19 and 20 show that the *r*-process $[Eu/O]_r$ and $[Eu/Mg]_r$ ratios in the bulk of Sgr stars are enhanced by ∼0.35 dex relative to the Galactic thin and thick disks. This is confirmed by the SM02/MS05 and Bonifacio et al. (2000) Sgr abundances.

How could the *r*-process $[Eu/O]_r$ ratios be so consistent in the Galactic disk but enhanced in the Sgr? We suggest that these $[Eu/O]_r$ enhancements result from a paucity of the most massive SNe II progenitor stars (which dominate oxygen production), and that the *r*-process is produced mostly in SNe II with masses lower than the average O and Mg producers. This paucity of the most massive high-mass stars could be due to either a steep massive-star IMF or a "top-light" SN mass function missing the upper mass range.

Abundance studies of extreme metal-poor MW halo stars indicate that there exists a large range of *r*-process yields from SNe II and that the bulk of the *r*-process elements were produced in a rare SNe II sub-type, at most only a few percent of all SNe II (e.g., McWilliam et al. 1995; Sneden et al. 1996; McWilliam 1998; McWilliam & Searle 1999; Fields et al. 2002).

We do not yet know the controlling factor, or factors, responsible for this rare, *r*-process, SNe II sub-type. However, the distinctly different $[Eu/O]_r$ ratios in Sgr and MW disks show that there is a systematic difference in one or more characteristics of the SNe II between these two systems. While angular momentum of the SNe II progenitor and binary membership might play a role in *r*-process production, we think it unlikely that these parameters differ significantly between the MW disks and Sgr. Similarly, metallicity is probably not the parameter mainly responsible for our $[Eu/O]_r$ result, because our Sgr stars and the MW thick-disk sample share a similar metallicity range. However, it seems possible that metallicity could play a role in modulating *r*-process yields, in general. On the other hand, the mass function of SNe II progenitors could well play a role in total *r*-process production and could reasonably differ between the MW disk and Sgr.

Under the assumption that the *r*-process yields are sensitive to the SNe II progenitor masses, the enhanced $[Eu/O]_r$ ratio indicates that the mass function of SNe II progenitors is more strongly weighted toward the mass of the *r*-process-producing SNe II in Sgr than in the MW disk. For example, if *r*-process-producing SNe II are predominantly lower mass, then $[Eu/O]_r$ enhancement would occur if the IMF is weighted to lower mass SNe II progenitors (i.e., a steep upper-end IMF slope or an upper mass cutoff).

The enhanced $[Eu/O]_r$ ratios, alone, cannot determine whether the IMF is steeper or shallower than Salpeter; however, the fact that oxygen is produced preferentially in high-mass SNe II suggests a steeper IMF in Sgr, i.e., with a paucity of high-mass stars. Additional evidence for such a "top-light" IMF in Sgr includes the deficiencies of hydrostatic elements O, Na, Mg, Al, and Cu relative to explosive elements Si, Ca, and Ti, consistent with muted nucleosynthesis contribution from SNe II compared to SNe Ia. The IGIMF has been predicted to be steeper in dwarf galaxies, like Sgr (e.g., Weidner & Kroupa 2005; Kroupa et al. 2011; see also Oey 2011). The reason is that dwarf galaxies have, by definition, less gas mass and lower mass molecular clouds than normal size galaxies, and as a result they are less efficient at producing the highest mass stars. Kroupa et al. (2011) also predicted a metallicity dependence of the IGIMF slope, which they expected to steepen with increasing metallicity.

Thus, the measured enhanced $[Eu/O]_r$ ratios lead to two interesting conclusions: (1) that *r*-process SNe II are lower mass

than the typical oxygen-producing and magnesium-producing SNe II, and (2) that either the massive-star IMF in Sgr was steeper than the MW disk, or there was a cutoff in the upper-end IMF, such as might be expected from Weidner & Kroupa (2005) and Oey (2011) IGIMF expectations.

If these conclusions are correct, then other dwarf galaxies should also show enhanced $[Eu/O]_r$ and $[Eu/Mg]_r$ ratios, since they too should possess IGIMFs steeper than the Salpeter value. Stars in Fornax (Letarte et al. 2010; Letarte 2013, unpublished), the LMC (Mucciarelli et al. 2008, 2010; Andrievsky et al. 2001; see also Van der Swaelmen et al. 2012), and IC 1613 (Tautvaišienė et al. 2007) show similar enhancements in $[Eu/O]_r$ and $[Eu/Mg]_r$ to those in Sgr. However, the relatively metal-poor dwarf galaxies Sculptor (Shetrone et al. 2003; Geisler et al. 2005) and Carina (Shetrone et al. 2003; Venn et al. 2012) do not share these enhancements. This non-uniform behavior might be explained by the predicted metallicity dependence of the IGIMF. Systematic measurement error in the Eu abundances of metal-rich stars seems unlikely, as the same problem would have occurred in MW disk red giants, but this is not seen.

4.9. Alternative Scenarios?

We have found that the declining [O/Fe] and $[Eu/Fe]_r$ trends with [Fe/H] in Sgr cannot both be explained by the late addition of Fe from delayed SNe Ia; two mechanisms are necessary. We have proposed a top-light or steep IMF in Sgr to reduce the abundances of the hydrostatic (O, Mg, Na, Al, Cu) and explosive (Si, Ca, Ti) element families; the [Eu/Fe]*r* trend could then be explained by the assumed delayed addition of Fe from SNe Ia, following the Tinsley (1979) scenario. If this is correct, then Sgr and the MW thick disk must have similar SFR, because the $[Eu/Fe]_r$ trend is similar in both systems; this may not be an unreasonable assumption, based on approximate age ranges of thick-disk and Sgr populations.

An alternative idea is that the hydrostatic and explosive element family is deficient, relative to Fe, due to a low SFR and extra Fe from SNe Ia in Sgr, following Tinsley (1979) and Matteucci & Brocato (1990), with the $[Eu/Fe]_r$ decline due to metallicity-dependent *r*-process yields.

The problem with this idea is that the Sgr and MW $[Eu/Fe]_r$ trends are very similar, yet the time-delay mechanism suggests more SNe Ia Fe in Sgr than in the MW. To accomplish this requires that the extra SNe Ia Fe in Sgr is accompanied by extra Eu production, exactly enough to make the Sgr and MW $[Eu/Fe]_r$ trends with [Fe/H] look similar. The *r*-process would be made by both SNe Ia and SNe II in this model, which may be difficult to understand in light of the large dispersion of $[Eu/Fe]_r$ in the metal-poor halo (e.g., McWilliam et al. 1995), indicating that the *r*-process is made in only a few percent of all SNe. However, this mechanism faces the fatal question of how the Sgr SNe Ia at $[Fe/H] = -0.5$ dex, say, know to make extra Eu, but the MW SNe Ia at the same metallicity do not make this extra Eu. This seems impossible.

This particular alternate scenario: where the Sgr hydrostatic X/Fe ratios were reduced by delayed SNe Ia Fe production at low SFR with Eu/Fe declining due to metal-dependent yields, and similar to the MW disk, introduces more problems than it solves.

In the context of the time-delay scenario, it seems much more reasonable to explain our measured abundance ratios by appealing to an IMF deficient in the most massive SNe II progenitors with the *r*-process located in lower mass SNe II, for which other evidence and arguments already exist.

We emphasize that metal-dependent *r*-process yields can be made consistent with our Sgr measurements and the MW if the time-delay mechanism is abandoned. In such a model hydrostatic, explosive, and *r*-process trends with [Fe/H] would all largely result from metallicity-dependent effects. This possibility will be discussed in more detail in a forthcoming paper.

5. THE CHEMICAL EVOLUTION OF Sgr

Various element abundance ratios provide clues to the chemical evolution of Sgr. The simplest diagnostic is [Fe/H], often incorrectly referred to as the "metallicity." In Sgr the mean [Fe/H] is near −0.5 to −0.7 dex (Cole 2001; Bellazzini et al. 2008; Siegel et al. 2007), much lower than the thin disk of the MW.

The low average [Fe/H] in Sgr may be due to significant mass loss during its evolution, which truncated chemical enrichment before complete conversion of the gas into stars could occur. A similar gas-loss mechanism was proposed by Hartwick (1976) to explain the low average [Fe/H] of the MW halo. Also, Kirby et al. (2011) required significant outflows to understand the mean metallicities of a sample of Local Group dwarf galaxies.

Presumably, outflows are more likely in low-mass galaxies, like Sgr, than the MW, because the relatively shallow gravitational potential well would permit more high-velocity SN ejecta to leave than for massive galaxies. However, tidal stripping by interaction with the MW must also have been an important gas-loss mechanism for Sgr, as evidenced by the prominent stellar tidal tails. Sgr contains almost no gas today.

A variant on overall mass loss is selective mass loss, for example, energetic material from SNe Ia or SNe II ejecta is, presumably, more likely to be ejected from Sgr than the low-velocity ejecta from planetary nebulae (PNe). Thus, one might reasonably expect a larger chemical abundance signal from PNe in dwarf galaxies; indeed, this may be consistent with the enhanced *s*-process abundances in Sgr and other dwarf galaxies. In terms of overall metallicity, selective mass loss from SNe II and/or SNe Ia would lower the yield of metals per stellar generation and reduce the amount of gas to be recycled into stars; both mechanisms would result in a lower mean [Fe/H].

A low mean [Fe/H] can also result from a steep stellar IMF. In a closed-box model of chemical evolution, the average metallicity of the system after all the gas is consumed is equal to the yield (Searle & Sargent 1972), a ratio that is the mass of metals produced divided by the mass locked up in low-mass stars. A system with a steep IMF slope (i.e., with a relatively high frequency of low-mass dwarfs) will, therefore, have a smaller yield, and the mean metallicity will be lower than for a normal IMF slope. In other words, for a steep IMF slope more gas is locked up in low-mass stars, leaving fewer high-mass stars to produce the metals, and thus the final average metallicity is lower.

Why did the Sgr MDF turn over near $[Fe/H] = -0.6$ dex? Was it due to a loss of gas from the shallow gravitational potential of Sgr, or some self-limitation on the SFR, possibly due to gas heating from hot stars; or did the MDF turnover result from a low effective yield, as a consequence of a steep IMF slope, or the selective loss of metals, or from a low binary fraction, leading to fewer SNe Ia events?

In light of Sgr's low mass, perhaps the most natural answer to this question is that its low mean [Fe/H] is due to chemical evolution in the presence of significant gas loss, i.e., leaky-box evolution, as suggested by SM02 and MS05.

Our IMF diagnostics include the hydrostatic and explosively produced elements, O, Mg, Na, Al, Cu, Si, Ca, Ti, and Eu. As outlined earlier in this paper, the ratios of hydrostatic to explosive element abundances, and in particular the [Eu/O] and [Eu/Mg] ratios, indicate a deficit of high-mass SNe II, most likely due to a top-light IGIMF. This probably resulted from the limited amount of gas available in Sgr, which restricted the formation of the most massive molecular clouds, from which the most massive stars are born (e.g., Weidner & Kroupa 2005; Kroupa & Weidner 2003).

Given the similarity of the chemical abundance ratios in Sgr with the LMC, it is reasonable to suppose a similar origin for the measured abundance ratios, in which case the LMC should also suffer from a top-light IGIMF. While the IMF slopes for clusters in the LMC are close to the Salpeter value seen in the MW (e.g., Massey 2003), the IMF derived from the measured current mass function of LMC field stars, a measure of the IGIMF, shows steep slopes, $\Gamma \sim -4$, above $1\,M_{\odot}$ (Gouliermis et al. 2006; Massey et al. 1995a), consistent with a top-light IGIMF. A caveat is that measured mass functions for field stars more massive than $\sim 1\,M_{\odot}$ require corrections to account for evolved stars and past star formation, in order to estimate the IMF.

We note that IMF slopes for MW field stars are also steep for masses $1\,M_{\odot} < M < 4\,M_{\odot}$, similar to the LMC values (e.g., Reid et al. 2002); however, we know of no MW measurements for the field-star IMF above $4\,M_{\odot}$. At present it is not possible to say whether the measured IMF slope for massive stars in the LMC field is steeper than the MW; see reviews by Massey (2003), Elemgreen (2004), Kroupa et al. (2011), and Scalo (2005) for further discussion. For the SMC field-star IMF Lamb et al. (2013) found a slope significantly steeper than Salpeter, at $\Gamma = -2.3 \pm 0.4$, for masses above $\sim 7\,M_{\odot}$; however, in the lowest two mass bins the slope was consistent with the Salpeter IMF slope. Numerical experiments by Lamb et al. (2013) showed that star formation corrections would most likely not affect the measured field-star IMF slopes. Thus, for the SMC a steep IMF is also indicated.

A comparison of the OB associations in M31 and the Local Group dwarf galaxy NGC 6822, by Massey et al. (1995b), showed that NGC 6822 OB associations have significantly fewer OB stars, with luminosities much less than in M31. This provides a crude comparison of the IGIMFs for the two galaxies and is consistent with, but does not prove, the existence of a top-light IGIMF in NGC 6822.

We conclude that there is mounting evidence that Local Group dwarf galaxies actually do possess steep IGIMF slopes, qualitatively consistent with the chemical abundance ratios measured in this work. However, the interpretation is complicated by necessary corrections and the fact that field stars in the MW disk also possess a steep present-day IMF slope.

As mentioned earlier, steep IGIMF slopes have been predicted for dwarf galaxies (e.g., Weidner & Kroupa 2005) where there is insufficient gas to form the most massive molecular clouds and hence the most massive stars. If this is true, then one should expect steep IMFs to occur whenever a system runs low on gas, such as in the presence of strong outflows, or simply gas consumption due to star formation. In the latter case, there will be relatively little star formation, and the IMF steepening will occur after the peak of the MDF. Indeed, it might be generally expected that the IMF slope will be steeper in the high-metallicity tail of the MDF. In this regard, it is interesting that the MW disk [Mg/Ca] ratios decline with increasing [Fe/H], although this might be due to increasing Ca from SNe Ia.

The large *s*-process enhancements in Sgr, such as [La/Fe], are evidence of the importance of low-mass AGB stars in the chemical evolution of this galaxy. This might be used to argue for a steep IGIMF slope, to low masses, in Sgr. However, the [La/Y] ratios in Sgr show, very clearly, that low-metallicity AGB stars produced the neutron-capture abundance patterns seen at high metallicity. Unsurprisingly, there was not instantaneous recycling of material in Sgr. The [La/Y] ratios show that the evolved low-metallicity stars from the peak of the [Fe/H] distribution function dominated the later evolution. Here we follow the suggestion of SM02 and MS05: that outflows, or a leaky-box scenario, caused the [La/Y] ratios of the metal-poor Sgr stars to dominate at high [Fe/H]. At any time, the gas was dominated by the ejecta from the peak of the metallicity function, near [Fe/H] $= -0.6$ dex, but due to progressively lower mass stars.

Our very low [Rb/Zr] ratios suggest that $2\,M_{\odot}$ AGB stars, with [Fe/H] ~ -0.6, dominated the chemical composition of the Sgr gas at [Fe/H] ~ -0.1 dex. Because the AGB *s*-process nucleosynthesis predictions of Cristallo et al. (2009, 2011) and Bisterzo et al. (2010) produce the very low [Rb/Zr] ratios seen in Sgr only for [Fe/H] above -1 dex, the source of the AGB material cannot have been from a population with lower metallicity, such as a metal-poor halo or M54, which has [Fe/H] ~ -1.8 dex. Thus, the region of Sgr studied here was likely self-enriched without significant inflow of metal-poor gas from other parts of the galaxy.

In summary, the abundance ratios measured here, and in other studies of Sgr, indicate chemical evolution of a system with a top-light IMF in the presence of outflows. The outflows are mainly responsible for the low mean metallicity of Sgr and cause a steady reduction in the population with increasing time and metallicity. Thus, ejecta from the relatively small metal-rich population are overwhelmed by nucleosynthesis products of the old [Fe/H] ~ -0.6 AGB stars. The top-light IMF results in abundance deficiencies of hydrostatic elements, like O, Mg, Na, Al, and Cu, but smaller deficiencies of explosive αs, like Si, Ca, and Ti. The [Eu/Fe] trend is similar to the MW disk; if we assume the time-delay paradigm of Tinsley (1979), this suggests that the SFR in Sgr was similar to the MW disk.

A test of this leaky-box scenario, in which the metal-rich composition was dominated by the products of metal-poor stars, may be facilitated by the trend of [Mn/Fe] with [Fe/H]. If metal-poor SNe Ia, following a significant time delay, contribute iron-peak elements to the metal-rich Sgr gas, then deficient [Mn/Fe] ratios are expected. Currently, there is dispersion in the reported [Mn/Fe] ratios from different Sgr abundance studies, so further investigation is required.

6. SUMMARY AND CONCLUSIONS

We have performed a high-resolution abundance analysis of three stars on the faint RGB toward M54. This giant branch has previously been shown to belong to Sgr, kinematically and chemically distinct from M54.

Our measurements indicate [Fe/H] values of -0.49, -0.39, and -0.09 dex for our three stars, consistent with previous measurement of the [Fe/H] distribution in Sgr. Our velocity dispersion is more consistent with the Sgr value indicated by Bellazzini et al. (2008) and less consistent with M54 kinematics; however, with only three points we can make no strong conclusion regarding the velocity dispersion of our stars.

Our detailed chemical abundance ratios are consistent with previous studies of stars in Sgr: deficient [α/Fe] ratios, particularly [O/Fe] and [Mg/Fe], suggest relatively less enrichment by the most massive SNe II; significant deficiencies of [Na/Fe], [Al/Fe], and [Cu/Fe] also indicate a paucity of ejecta from more massive SNe II; enhancements of neutron-capture elements, made by the *s*-process, show enrichment by AGB stars, with the enhanced heavy-to-light *s*-process ratio (e.g., [La/Y]) consistent with low-metallicity AGB nucleosynthesis. These unusual abundance ratios provide further evidence that our program stars are, indeed, members of Sgr. Furthermore, our results and those of S07 show no evidence of an Na–O abundance anti-correlation, seen in most globular clusters, which supports the conclusion that our stars are not members of M54.

We do not confirm the deficient [V/Fe] ratios found by Sbordone et al. (2007), nor the Na enhancements found for the metal-rich Sgr stars by Carretta et al. (2010). We believe these earlier claims to be spurious, arising from systematic errors in these other studies, perhaps due to model atmosphere problems and blends. However, given the spatial distance between the S07 sample and those of C10 and SM02, it is possible that a chemical abundance gradient could have produced the putative vanadium deficiency claimed by S07.

We also do not confirm the $\sim$0.2 dex lower-than-normal [Mn/Fe] values claimed by McWilliam et al. (2003); in this work we find that the [Mn/Fe] trend resembles the MW disk and halo. This difference may be due to the uncertainties involved with the absolute abundance technique of SM02 and McWilliam et al. (2003) combined with the paucity of photometric and reddening information available, which made it difficult to constrain the atmosphere parameters of their stars. Additionally, in SM02 the [Mn/Fe] uncertainties were increased by the discrepancy between published solar photospheric and meteoritic values. While we believe that the techniques employed in this work are superior to SM02 and McWilliam et al. (2003), it is still possible that the [Mn/Fe] discrepancy could be due to the relatively low S/N of the current spectra. Thus, it is necessary to revisit the [Mn/Fe] trend in Sgr with a more extensive and higher S/N chemical abundance study. This is particularly relevant following the discovery of Mn deficiencies in ω Cen by Cunha et al. (2010).

Although our neutron-capture element abundances show the same character as previous studies by Smecker-Hane & McWilliam (2002) and Sbordone et al. (2007), there are differences between the results. In this work the [La/Y] ratios are significantly higher than those of SM02, especially at [Fe/H] = $-$0.09 dex, for which our value is higher by 0.5 dex; however, our results are slightly lower than the [La/Y] values found by B00 and S07 (see Figures 14 and 15). Because of limited spectral coverage, SM02 were forced to use less-than-optimal Y II lines, including the line at 5402.8 Å, which is blended and required spectrum synthesis to account for the contamination. For this reason, we did not employ this Y II line in the current work; it is possible that the blended Y II lines in SM02 might explain the discrepancy with all other studies. A comparison of published [La/Y] ratios for Sgr, in Figure 14, indicates a steep increase of [La/Y] with increasing [Fe/H]. Whether [La/Y] is flat with [Fe/H], as found by SM02, or steeply rising has implications for the chemical evolution of Sgr; therefore, this [hs/ls] ratio requires further investigation.

Notwithstanding, the prevailing [La/Y] versus [La/H] trend in Figure 15 shows that the locus of the maximum theoretically predicted [La/Y] AGB yields, from Cristallo et al. (2011), falls $\sim$0.3 dex below the measured values for Sgr from this work, B00, and S07. This may indicate a factor of two underestimate for the Standard Pocket, ST, of hydrogen ingested into the inter-shell region of the AGB star, in the theory employed by Cristallo and collaborators (going back to Gallino et al. 1998). Curiously, the SM02 [La/Y] ratios are not in conflict with theoretical AGB *s*-process nucleosynthesis predictions. Another difficulty is that the Cristallo et al. (2011) [hs/ls] predictions showed good agreement with chemical abundance measurements of *s*-process-enhanced stars in the MW. Thus, if the high [La/Y] ratios in Sgr prevail, then it may appear that AGB *s*-process is different in the MW and Sgr. It seems possible that such differences could be due to the distinct chemical composition of these two galaxies (e.g., O, Mg, and *s*-process). However, an alternate possibility is that the MW comparisons used by Cristallo et al. (2011) did not measure the final AGB [hs/ls] ratios, because the MW stars either were not-yet-dead AGB stars or involved mass-transfer from AGB stars before the terminal *s*-process ratios were achieved.

Small discrepancies exist for [La/Eu] in Sgr, which are slightly higher here than in SM02 (see Figure 13). However, the differences are well within the measurement uncertainties; we suspect that this is due to slightly high Eu abundances in SM02, possibly as a result of the gravities employed. We prefer the [La/Eu] results presented here over SM02.

We find that the [O/Fe] trend with [Fe/H] is deficient by 0.4 dex in Sgr, relative to the MW disk, while the trend of [Eu/Fe] and particularly the pure *r*-process [Eu/Fe]$_r$ (i.e., corrected for *s*-process Eu) shows no deficiency compared to the MW disk. Thus, it is not possible to explain the premature decline in [O/Fe] with [Fe/H] by the addition of extra iron in the SNe Ia time-delay scenario of Tinsley (1979) without then predicting large deficiencies in the trend of [Eu/Fe]$_r$ with [Fe/H]. A more reasonable explanation is that the deficient [O/Fe] ratios resulted from a paucity of the highest mass SNe II in Sgr; this modification of the IMF of SNe II progenitors is qualitatively consistent with the measured ratios of hydrostatic to explosive elements in Sgr.

We also found 0.3–0.4 dex enhancements in the *r*-process-corrected [Eu/O]$_r$ and [Eu/Mg]$_r$ ratios in Sgr relative to the MW disks. This result simultaneously indicates that the most massive SNe II progenitors were deficient in Sgr (i.e., either a top-light IMF or a steep IMF) and that the *r*-process SNe II are of lower mass than the oxygen-producing SNe II. Since oxygen is produced in SNe II of $\sim$30 $M_\odot$ and above (e.g., Woosley & Weaver 1995), *r*-process SNe II are less massive than $\sim$30 $M_\odot$, in qualitative agreement with some theoretical predictions, e.g., Wanjo et al. (2003). Deficiencies in the abundances of other elements made by SNe II (e.g., Al, Na, the α-elements, and Cu) are qualitatively consistent with a top-light or steep IMF; however, the interpretation is complicated by the unknown nucleosynthetic contribution from SNe Ia, which depends on age and SFR.

Similar enhancements of [Eu/O] and/or [Eu/Mg] ratios, and differences between [O/Fe] or [Mg/Fe] and [Eu/Fe] trends, have been seen in other dwarf galaxies, such as the LMC, Fornax, and IC 1613; this indicates that the same deficit of high-mass SNe II, suggesting a top-light or steep IMF, has occurred in those systems. Such steep galaxy IGIMF slopes in dwarf galaxies have been predicted (e.g., Weidner & Kroupa 2005). The metal-poor dwarf galaxies studied to date, e.g., Sculptor and Carina, do not show enhanced [Eu/O] and [Eu/Mg] ratios. This might be consistent with the predicted

metallicity dependence of the IGIMF by Kroupa et al. (2011). Our *r*-process $[Eu/O]_r$ and $[Eu/Mg]_r$ measurements provide an important observational constraint on both the site of the *r*-process and the IMF of Sgr.

We report the first abundance measurement of Rb and the [Rb/Zr] ratio in Sgr. While all three of our stars have very low [Rb/Zr] ratios, our most metal-rich star, 247 at [Fe/H] = −0.09 dex, has a remarkably low value, at [Rb/Zr] = −0.72 dex; this is probably the lowest value ever reported. Theoretical predictions show that this ratio could have been produced by AGB stars with [Fe/H] $\gtrsim -1$, but not from AGB stars with [Fe/H] characteristic of M54 or a metal-poor halo.

Comparison with the theoretical predictions indicates that the low [Rb/Zr] ratios measured in this work were probably produced by low-mass AGB stars ($\lesssim 2\ M_\odot$), via the $^{13}C(\alpha,n)^{16}O$ neutron source, in the main Sgr population with [Fe/H] peak near −0.6 dex. Thus, the role of intermediate-mass AGB stars, relative to low-mass AGB stars, was much diminished in Sgr compared to the MW disk and halo.

Although published yields are insufficient to place tight constraints on the AGB masses indicated by the [Rb/Zr] ratios, our measurements are consistent with published yields for AGB stars in the range 1.3–2.0 $M_\odot$. This suggests a timescale consistent with the ages of the 4–6 Gyr old and the 2.3 Gyr old sub-populations in Sgr, identified by Siegel et al. (2007).

It is interesting that the [Rb/Zr] ratios in our sample of three stars are linearly dependent on the [Fe/H]; while this may simply result from low-number statistics, it suggests that there was either a gradual decrease in [Rb/Zr], due to a steady increase in AGB metallicities, or a decrease in the mean mass of the AGB stars. It is also possible that the steady decline of [Rb/Zr] with [Fe/H] is due to dilution of metal-poor, high-[Rb/Zr] material with metal-rich, low-[Rb/Zr] ejecta from AGB stars. More data are required to investigate these possibilities.

The only known stellar population with similar low [Rb/Zr] values is ω Cen (Smith et al. 2000). It is clear that, once again, Sgr and ω Cen are chemically similar, suggesting similar chemical evolution histories. It is also clear that these systems provide useful grounds for testing theoretical models of the *s*-process in low-mass AGB stars.

Andrew McWilliam would like to thank George Preston, Sara Bisterzo, and Sergio Cristallo for useful conversations. We also express deep gratitude to Carnegie Observatories librarian John Grula for his efforts in obtaining copies of papers with atomic data critical to this work. Thanks also to Kim Venn and the referee, Piercarlo Bonifacio, for useful comments.

APPENDIX A

ERROR ANALYSIS

In this work we have computed the uncertainties for our abundances following the method outlined in the Appendix of McWilliam et al. (1995); however, we have extended the formulae to include uncertainties arising from the model atmosphere metallicity. We present Equations (A1)–(A5) employed here:

$$\sigma(\bar{\varepsilon})^2 = \sigma_r(\bar{\varepsilon})^2 + \left(\frac{\partial\bar{\varepsilon}}{\partial T}\right)^2\sigma_T^2 + \left(\frac{\partial\bar{\varepsilon}}{\partial g}\right)^2\sigma_g^2 + \left(\frac{\partial\bar{\varepsilon}}{\partial\xi}\right)^2\sigma_\xi^2 + \left(\frac{\partial\bar{\varepsilon}}{\partial[\mathrm{M/H}]}\right)^2\sigma_{[\mathrm{M/H}]}^2 + 2\left[\left(\frac{\partial\bar{\varepsilon}}{\partial T}\right)\left(\frac{\partial\bar{\varepsilon}}{\partial g}\right)\sigma_{Tg} + \left(\frac{\partial\bar{\varepsilon}}{\partial T}\right)\left(\frac{\partial\bar{\varepsilon}}{\partial\xi}\right)\sigma_{T\xi} + \left(\frac{\partial\bar{\varepsilon}}{\partial g}\right)\left(\frac{\partial\bar{\varepsilon}}{\partial\xi}\right)\sigma_{g\xi} + \left(\frac{\partial\bar{\varepsilon}}{\partial[\mathrm{M/H}]}\right)\left(\frac{\partial\bar{\varepsilon}}{\partial T}\right)\sigma_{T[\mathrm{M/H}]}\right], \quad \text{(A1)}$$

where $\sigma_r(\bar{\varepsilon})$ is the uncertainty on the average abundance due to random errors, σ_X^2 is the variance of atmosphere parameter *X*, and σ_{XY} is the covariance between two atmosphere parameters, *X* and *Y*. For the random component, we have employed the measured error on the average abundance for species with multiple lines to estimate $\sigma_r(\bar{\varepsilon})$; this will include the effects of unaccounted blends. For species represented by only one line we computed $\sigma_r(\bar{\varepsilon})$ from the uncertainty in the measured EW, according to Equations (A2) and (A3), below. In principle, Equations (A2) and (A3) could be employed to compute $\sigma_r(\bar{\varepsilon})$ for all species, starting from the S/N of the observed spectrum. Note that Equation (A3) could be extended to include other sources of uncertainty on individual line abundances, for example, due to error in the adopted damping constants:

$$\frac{1}{\sigma_r(\bar{\varepsilon})^2} = \sum^{N_{\mathrm{lines}}}\frac{1}{\sigma_i(\varepsilon)^2}, \quad \text{(A2)}$$

$$\sigma_i(\varepsilon)^2 = \left(\frac{\partial\varepsilon_i}{\partial\mathrm{EW}}\right)^2\sigma_{\mathrm{EW}_i}^2 + \sigma_{\log gf_i}^2. \quad \text{(A3)}$$

The uncertainty on the abundance ratio [*A*/*B*] is given by

$$\sigma([A/B])^2 = \sigma_{\varepsilon(A)}^2 + \sigma_{\varepsilon(B)}^2 - 2\sigma_{A,B}, \quad \text{(A4)}$$

where the covariance between abundances of species *A* and *B*, $\sigma_{A,B}$ is given by

$$\sigma_{A,B} = \left(\frac{\partial\bar{\varepsilon}_A}{\partial T}\right)\left(\frac{\partial\bar{\varepsilon}_B}{\partial T}\right)\sigma_T^2 + \left(\frac{\partial\bar{\varepsilon}_A}{\partial g}\right)\left(\frac{\partial\bar{\varepsilon}_B}{\partial g}\right)\sigma_g^2 + \left(\frac{\partial\bar{\varepsilon}_A}{\partial\xi}\right)\times\left(\frac{\partial\bar{\varepsilon}_B}{\partial\xi}\right)\sigma_\xi^2 + \left(\frac{\partial\bar{\varepsilon}_A}{\partial[\mathrm{M/H}]}\right)\left(\frac{\partial\bar{\varepsilon}_B}{\partial[\mathrm{M/H}]}\right)\sigma_{[\mathrm{M/H}]}^2 + \left[\left(\frac{\partial\bar{\varepsilon}_A}{\partial T}\right)\left(\frac{\partial\bar{\varepsilon}_B}{\partial\xi}\right) + \left(\frac{\partial\bar{\varepsilon}_A}{\partial\xi}\right)\left(\frac{\partial\bar{\varepsilon}_B}{\partial T}\right)\right]\sigma_{T\xi} + \left[\left(\frac{\partial\bar{\varepsilon}_A}{\partial T}\right)\left(\frac{\partial\bar{\varepsilon}_B}{\partial g}\right) + \left(\frac{\partial\bar{\varepsilon}_A}{\partial g}\right)\left(\frac{\partial\bar{\varepsilon}_B}{\partial T}\right)\right]\sigma_{Tg} + \left[\left(\frac{\partial\bar{\varepsilon}_A}{\partial\xi}\right)\left(\frac{\partial\bar{\varepsilon}_B}{\partial g}\right) + \left(\frac{\partial\bar{\varepsilon}_A}{\partial g}\right)\left(\frac{\partial\bar{\varepsilon}_B}{\partial\xi}\right)\right]\sigma_{g\xi} + \left[\left(\frac{\partial\bar{\varepsilon}_A}{\partial T}\right)\left(\frac{\partial\bar{\varepsilon}_B}{\partial[\mathrm{M/H}]}\right) + \left(\frac{\partial\bar{\varepsilon}_A}{\partial[\mathrm{M/H}]}\right)\left(\frac{\partial\bar{\varepsilon}_B}{\partial T}\right)\right]\sigma_{T[\mathrm{M/H}]}. \quad \text{(A5)}$$

In these equations we include the covariance of [M/H] with T_{eff}, since [M/H] was based on the Fe I abundance, which is temperature dependent; however, we have omitted all other parameter covariances with [M/H]. Also, we ignore the possibility of covariance between EWs of species *A* and *B*, which holds for separated lines; however, if lines of *A* and *B* are blended together, an EW covariance could exist.

The sensitivity of the element abundances to model atmosphere parameters and the model atmosphere variances and covariances are necessary ingredients to Equations (A1)–(A5). From numerical experiments we have computed the dependence

Table 9
Abundance Sensitivity to Atmosphere Parameters

	Δ $T_{\rm eff}$		Δ log g		Δ ξ		Δ [M/H]	
	(+50 K)	(−50 K)	(+0.2 dex)	(−0.2 dex)	(+0.3 km s)	(−0.3 km s)	(+0.1 dex)	(−0.1 dex)
Fe I	−0.03	+0.02	+0.04	−0.04	−0.11	+0.13	+0.03	−0.01
Fe II	−0.11	+0.11	+0.17	−0.08	−0.07	+0.08	+0.08	−0.01
[O I][a]	+0.01	+0.00	+0.07	−0.05	−0.01	+0.02	+0.03	−0.02
Na I	+0.05	−0.04	+0.01	−0.01	−0.05	+0.07	+0.01	+0.01
Mg I	−0.02	+0.03	+0.05	−0.01	−0.06	+0.07	+0.03	+0.00
Al I	+0.03	−0.03	+0.01	+0.00	−0.04	+0.05	+0.01	+0.01
Si I	−0.06	+0.07	+0.09	−0.03	−0.04	+0.04	+0.05	+0.00
Ca I	+0.05	−0.05	+0.01	+0.00	−0.14	+0.18	+0.01	+0.00
Ti I	+0.07	−0.06	+0.02	−0.02	−0.20	+0.26	+0.02	−0.01
Ti II	−0.04	+0.03	+0.11	−0.08	−0.05	+0.05	+0.05	−0.03
V I	+0.07	−0.06	+0.03	−0.03	−0.18	+0.19	+0.02	−0.02
Mn I	+0.01	−0.00	+0.06	−0.03	−0.10	+0.12	+0.03	−0.01
Cu I	+0.00	+0.00	+0.08	−0.05	−0.08	+0.10	+0.05	−0.01
Rb I	+0.07	−0.07	+0.00	+0.00	−0.01	+0.01	+0.01	+0.00
Zr I	+0.08	−0.08	+0.03	−0.03	−0.18	+0.27	+0.02	−0.02
Y II	−0.01	+0.01	+0.09	−0.07	−0.03	+0.05	+0.05	−0.03
La II	+0.01	−0.01	+0.09	−0.08	−0.05	+0.05	+0.05	−0.03
Eu II	−0.01	+0.01	+0.10	−0.07	−0.03	+0.04	+0.05	−0.02

Note. [a] Oxygen abundances assume RGB carbon depletion of 0.2 dex. If ΔC = +0.10 dex, ΔO = +0.04 dex. If ΔC= −0.10 dex, ΔO = −0.03 dex.

Table 10
Atmosphere Parameter Variances and Covariances

Var./Covar.	Value
σ_T	47.0
σ_g	0.040
σ_ξ	0.02
$\sigma_{\rm [M/H]}$	0.024
σ_{Tg}	1.88
$\sigma_{T\rm [M/H]}$	1.105
$\sigma_{g\xi}$	−0.0011
$\sigma_{T\xi}$	0.00

Table 11
Abundance Ratio Uncertainties

	Atmosphere Uncertainties					
Ion	σ[X/H]	σ[X/Fe I]	σ[X/Fe II]	$\sigma_{\rm rand}$[X/H][a]	$\sigma_{\rm total}$[X/Fe I]	$\sigma_{\rm total}$[X/Fe II]
Fe I	0.02	...	0.06	0.023	0.03[b]	...
Fe II	0.07	0.06	...	0.105	...	0.13[b]
[O I]	0.02	0.03	0.09	0.033[c]	0.04	0.10
Na I	0.05	0.06	0.11	0.13	0.14	0.17
Mg I	0.02	0.01	0.05	0.015	0.02	0.05
Al I	0.03	0.04	0.10	0.035	0.05	0.11
Si I	0.05	0.03	0.03	0.065	0.07	0.07
Ca I	0.05	0.06	0.12	0.072	0.09	0.14
Ti I	0.07	0.08	0.15	0.064	0.10	0.16
Ti II	0.02	0.00	0.06	0.20	0.20	0.21
V I	0.08	0.08	0.14	0.057	0.10	0.15
Mn I	0.03	0.03	0.09	0.046	0.05	0.10
Cu I	0.03	0.03	0.09	0.096[c]	0.10	0.13
Rb I	0.07	0.08	0.14	0.01	0.08	0.14
Zr I	0.09	0.10	0.15	0.045	0.11	0.16
Y II	0.02	0.03	0.08	0.050	0.06	0.09
La II	0.04	0.05	0.10	0.092	0.10	0.14
Eu II	0.02	0.03	0.08	0.058[c]	0.07	0.10

Notes.
[a] For species with more than one measured line, random abundance errors, due to EW uncertainties, were adopted from the error on the mean abundances, derived from the dispersions in Table 7.
[b] Instead of $\sigma_{\rm total}$[X/Fe] we provide $\sigma_{\rm total}$[Fe/H] ratios.
[c] Random abundance errors for O, Cu, and Eu were computed from 1σ EW measurement uncertainties, based on the S/N for each pixel of each line, at 4.6, 4.2, and 7.0 mÅ, respectively.

of abundance on atmosphere parameters for all elements measured in star 242; the results are listed in Table 9.

In the evaluation of our abundance measurement uncertainties we first consider the effective temperature, $T_{\rm eff}$. The rms difference of the nine color $T_{\rm eff}$ values in Table 5 is 36 K, indicating an uncertainty of 26 K for each average color temperature. To this it was necessary to add, in quadrature, a 15 K uncertainty resulting from 0.03 mag uncertainty for the V-band photometry, common to all our colors, a 20 K uncertainty due to 0.02 mag reddening uncertainty for Sgr (Layden & Sarajedini 2000), the uncertainty on the Arcturus physical $T_{\rm eff}$ value of ±29 K (Koch & McWilliam 2008), and the uncertainty of ±7 K on the effective temperature of the Sun. These terms indicate a total 1σ $T_{\rm eff}$ uncertainty on our Sgr temperatures (relative to the solar temperature) of 47 K.

In this work we have adopted log g values from the BASTI isochrones, using the adopted $T_{\rm eff}$ and metallicity, [M/H], in an iterative differential abundance analysis. Our formal uncertainty in log g results, directly, from the temperature uncertainty. We computed the log g uncertainty from the slope of log g versus $T_{\rm eff}$ times σT; $\sigma(T) = 47$ K corresponds to $\sigma(\log g) = 0.040$ dex.

Because $T_{\rm eff}$ and our adopted log g values are correlated, it is necessary to include the covariance between these two parameters, σ_{Tg}, when evaluating the abundance uncertainties. The covariance between temperature and gravity, $\sigma_{\rm Tg}$, was computed using Equation (A6):

$$\sigma_{\rm Tg} = \langle \Delta g \Delta T \rangle = \left(\frac{\partial g}{\partial T} \right) \sigma_T^2, \qquad \text{(A6)}$$

where the gradient, $(\partial g/\partial T)$, was measured from the BASTI isochrone appropriate for star 242. Accordingly, we find $\sigma_{\rm Tg} = 1.88$. We remind the reader that covariances between atmosphere parameters depend on the method used to measure them. We

Table 12
hfs References

Ion	References
V I	Kopfermann, H., & Rasmussen, E. 1936, ZPhy, 98, 624
	Childs, W. J., Poulsen, O., Goodman, L. S., & Crosswhite, H. 1979, PhRvA, 19, 168
	Kurucz, R. L., unpublished (http://kurucz.harvard.edu/)
	Johnson, J. A., Ivans, I. I., & Stetson, P. B. 2006, ApJ, 640, 801
Mn I	Handrich, E., Steudel, A., & Walther, H. 1969, PhL, 29A, 486
	(components computed by R. L. Kurucz, http://kurucz.harvard.edu/)
Cu I	Cunha, K., Smith, V., Suntzeff, N. B., et al. 2002, AJ, 124, 379
	Biehl, D. 1976, PhD thesis, Univ. Kiel
Rb I	Daniel A. Steck, "Rubidium 85 D line Data," available online at
	http://steck.us/alkalidata (revision 2.1.4, 2010 December 23)
	Daniel A. Steck, "Rubidium 87 D line Data," available online at
	http://steck.us/alkalidata (revision 2.1.4, 2010 December 23)
	Banerjee, A., Das, A., & Natarajan, V. 2004, EL, 65, 172
Y II	Persson, J. R. 1997, ZPhyD, 42, 259
	Beck, D. R. 1992, PhRvA, 65, 1399
	Dinneen, T. P., Mansour, N. B., Kurtz, C., & Young, L. 1991, PhRvA, 43, 4824
	Villemoes, P., Arnesen, A., Heijkenskjöld, F., Kastberg, A., & Larsson, O. 1992,
	PhyS, 46, 45
Zr I	Chevalier, G., Gagné, J.-M., & Pianarosa, P. 1988, JOSAB, 5, 1492
	Chevalier, G., & Gagné, J.-M. 1986, OptCo, 57, 327
	Bouazza, S., Gough, D. S., Hannaford, P., & Wilson, M. 2002, JPhB, 35, 2397
	Gough, D. S., & Hannaford, P. 1988, OptCo, 67, 209
	McLean, R. J., Hannaford, P., & Larkins, P. L. 1993, OptCo, 102, 43
	Büttgenbach, S., Dicke, R., Gebauer, H., Kuhnen, R., & Träber, F. 1978, ZPhyA, 286, 125
La II	Lawler, J. E., Bonvallet, G., & Sneden, C. 2001, ApJ, 556, 452
	Furmann, B., Elantkowska, M., Stefańska, D., Ruczkowski, J., & Dembczyński, J.
	2008, JPhB, 41, 235002
	Furmann, B., Ruczkowski, J., Stefańska, D., Elantkowska, M., & Dembczyński, J.
	2008, JPhB, 41, 215004
Eu II	Lawler, J. E., Wickliffe, M. E., Den Hartog, E. A., & Sneden, C. 2001, ApJ, 563, 1075

have employed photometric temperatures and gravities with help from theoretical isochrones; $\sigma_{\rm Tg}$ would have been different for spectroscopically determined gravities and/or temperatures.

The standard error in the slope of the plot of [Fe I/H] versus EW for star 242 corresponds to a 1σ microturbulent velocity uncertainty of 0.02 km s^{-1}. Because we have employed a line-by-line differential analysis, the scatter in this slope is particularly small, since there is no dispersion due to uncertainties in gf values. For the covariance between gravity and microturbulent velocity, $\sigma_{g\xi}$, we estimated a maximum change in slope in the ϵ(Fe I) versus EW plot for a change in gravity of 0.2 dex, thus permitting calculation of $\langle \Delta g \Delta \xi \rangle$. Accordingly, we found $\sigma_{T\xi} = -0.0011$; this covariance estimate would have been larger had absolute gf values been used in the analysis. For $\sigma_{\rm [M/H]}$ we adopted the uncertainty in [Fe I/H], which is dominated by the uncertainty in $T_{\rm eff}$. Clearly, the exact chemical composition, among other variables, could affect our choice of model atmosphere metallicity; however, we note that increasing $\sigma_{\rm [M/H]}$ to 0.06 dex made a negligible difference to the total error budget. For the temperature-metallicity covariance, $\sigma_{T\,\rm [M/H]}$, we employed the abundance sensitivities in Table 9, resulting in a covariance of 1.105 K dex. Finally, we could see no significant covariance between temperature and microturbulent velocity, so this has been assumed to be zero in this work. Our resultant standard errors and covariances are summarized in Table 10.

When the variances and covariances from Table 10 are inserted into Equations (A1)–(A3) and combined with the random errors of Table 7 to estimate the EW measurement uncertainties, we compute the abundance uncertainties, relative to H, Fe I, and Fe II, as shown in Table 11. It is notable, and unexpected, that the ratios [X/Fe II] are always inferior to [X/Fe I] in Table 11, even for [O I], Ti II, and other ionized lines; we assume that this is because our stellar temperatures are cool enough that Fe I is the dominant ionization stage, unlike the red giant stars a few hundred degrees hotter.

Caveats regarding our treatment of the abundance measurement uncertainty are related to systematic effects, particularly the omission of physics in the one-dimensional LTE model atmospheres and the use of LTE radiative transfer. Improvements could include 3D hydrodynamical atmospheres with non-LTE radiative transfer. However, it is hoped that our differential abundance technique has minimized the deviations from these omissions; also, abundance corrections from these two effects tend to have opposite sign, canceling to some degree. We also warn that we have assumed that our stars are on the RGB, rather than AGB, when selecting the gravity for our model atmospheres. On the RGB our stars have log g values only 0.07 dex higher than the AGB. However, if the mass-loss prescription used in the BASTI isochrones is greatly different, this gravity difference may be somewhat larger or smaller. Another issue is that we have employed scaled-solar composition model atmospheres, from the Kurucz grid, whereas our analysis shows that elements that are important electron donors, namely, Na, Mg, Al, and Si, are deficient in all our stars. A simple calculation for locations in one of our model atmospheres indicates that N_e should be reduced by $\sim$30%, or $\sim$0.1 dex. Such changes in N_e would reduce the abundances of Fe II, Ti II, and [O I] lines. A more complete propagation of errors would consider this effect. For this reason,

although or results suggest a reduction in the measurement error for [O I] and Ti II by ratioing with Fe I abundances, we prefer to ratio with Fe II abundances, in order to subtract out systematic abundance errors due to inappropriate N_e in the model atmospheres.

APPENDIX B

REFERENCES

Table 12 lists the source references for the hfs constants employed in the calculations in this work.

REFERENCES

Allende Prieto, C., Barklem, P. S., Lambert, D. L., & Cunha, K. 2004, A&A, 420, 183
Alonso, A., Arribas, S., & Martinez-Roger, C. 1999, A&AS, 140, 261
Andersen, J., Gustafsson, B., & Lambert, D. L. 1984, A&A, 136, 65
Andrievsky, S. M., Kovtyukh, V. V., Korotin, S. A., Spite, M., & Spite, F. 2001, A&A, 367, 605
Andrievsky, S. M., Spite, M., Korotin, S. A., et al. 2008, A&A, 481, 481
Arlandini, C., Käppeler, F., Wisshak, K., Gallino, R., Lugaro, M., Busso, M., & Straniero, O. 1999, ApJ, 525, 886
Arnett, W. D. 1971, ApJ, 166, 153
Bellazzini, M., Ibata, R. A., Chapman, S. C., et al. 2008, AJ, 136, 1147
Bensby, T., Feltzing, S., Lundström, I., & Ilyin, I. 2005, A&A, 433, 185
Bergemann, M. 2011, MNRAS, 413, 2184
Bergemann, M., & Gehren, T. 2007, A&A, 473, 291
Bessell, M. S. 1979, PASP, 91, 589
Bisterzo, S., Gallino, R., Pignatari, M., et al. 2004, MmSAI, 75, 741
Bisterzo, S., Gallino, R., Straniero, O., Cristallo, S., & Käppeler, F. 2010, MNRAS, 404, 1529
Bisterzo, S., Gallino, R., Straniero, O., Cristallo, S., & Käppeler, F. 2011, MNRAS, 418, 284
Blackwell, D. E., Shallis, M. J., & Simmons, G. J. 1982, MNRAS, 199, 33
Bonifacio, P., Hill, V., Molaro, P., et al. 2000, A&A, 359, 663
Bonifacio, P., Sbordone, L., Marconi, G., Pasquini, L., & Hill, V. 2004, A&A, 414, 503
Brown, J. A., Sneden, C., Lambert, D. L., & Dutchover, E. 1989, ApJS, 71, 293
Brown, J. A., Wallerstein, G., & Gonzalez, G. 1999, AJ, 118, 1245
Brown, J. A., Wallerstein, G., & Zucker, D. 1997, AJ, 114, 180
Burris, D. L., Pilachowski, C. A., Armandroff, T. E., et al. 2000, ApJ, 544, 302
Busso, M., Gallino, R., & Wasserburg, G. J. 1999, ARA&A, 37, 239
Busso, M., Straniero, O., Gallino, R., & Abia, C. 2004, in Symp. Carnegie Obs., Origin and Evolution of the Elements, ed. A. McWilliam & M. Rauch (Carnegie Observatories Astrophysics Series; Cambridge: Cambridge Univ. Press), 67
Carlsson, M., Rutten, R. J., Bruls, J. H. M. J., & Shchukina, N. G. 1994, A&A, 288, 860
Carretta, E., Bragaglia, A., Gratton, R. G., et al. 2009, A&A, 505, 117
Carretta, E., Bragaglia, A., Gratton, R. G., et al. 2010, A&A, 520, 95 (C10)
Casagrande, L., Ramírez, I., Meléndez, J., Bessell, M., & Asplund, M. 2010, A&A, 512, 54
Castelli, F., Gratton, R. G., & Kurucz, R. L. 1997, A&A, 318, 841
Cescutti, G., Matteucci, F., Lanfranchi, G. A., & McWilliam, A. 2008, A&A, 491, 401
Cescutti, G., Matteucci, F., McWilliam, A., & Chiappini, C. 2009, A&A, 505, 605
Chieffi, A., & Limongi, M. 2006, in "Proceedings of the International Symposium on Nuclear Astrophysics" Nuclei in the Cosmos IX. (Geneva: CERN), 250
Chou, M.-Y., Cunha, K., Majewski, S. R., et al. 2010, ApJ, 708, 1290
Cohen, J. G. 2004, ApJ, 127, 1545
Cole, A. 2001, ApJL, 559, L17
Condon, E. U., & Shortly, G. H. 1935, Theory of Atomic Spectra (Cambridge: Cambridge Univ. Press)
Conti, P., Greenstein, J. L., Spinrad, H., Wallerstein, G., & Vardya, M. S. 1967, ApJ, 148, 105
Cristallo, S., Piersanti, L., Straniero, O., et al. 2011, ApJS, 197, 17
Cristallo, S., Straniero, O., Gallino, R., et al. 2009, ApJ, 696, 797
Cunha, K., Smith, V. V., Bergemann, M., Suntzeff, N. B., & Lambert, D. L. 2010, ApJ, 717, 333
Cunha, K., Smith, V. V., Suntzeff, N. B., et al. 2002, AJ, 124, 379
Da Costa, G. S., & Armandroff, T. E. 1995, AJ, 109, 2533
Edvardsson, B., Andersen, J., Gustafsson, B., et al. 1993, A&A, 275, 101
Elemgreen, B. G. 2004, MNRAS, 354, 367
Elias, J. H., Frogel, J. A., & Humphreys, R. M. 1985, ApJS, 57, 91
Feltzing, S., Fohlman, M., & Bensby, T. 2007, A&A, 467, 665
Fields, B. D., Truran, J. W., & Cowan, J. J. 2002, ApJ, 575, 845
Fulbright, J. P., McWilliam, A., & Rich, R. M. 2006, ApJ, 636, 821
Fulbright, J. P., McWilliam, A., & Rich, R. M. 2007, ApJ, 661, 1152
Gallino, R., Arlandini, C., Busso, M., et al. 1998, ApJ, 497, 388
García-Hernández, D. A. 2011, in ASP Conf. Ser. 445, Why Galaxies Care about AGB Stars II: Shining Examples and Common Inhabitants, ed. F. Kerschbaum, T. Lebzelter, & R. F. Wing (San Francisco, CA: ASP), 437
García-Hernández, D. A., García-Lario, P., Plez, B., et al. 2006, Sci, 314, 1751
Gehren, T., Shi, J. R., Zhang, H. W., Zhao, G., & Korn, A. J. 2006, A&A, 451, 1065
Geisler, D., Smith, V. V., Wallerstein, G., Gonzalez, G., & Charbonnel, C. 2005, AJ, 129, 1428
Gouliermis, D., Brandner, W., & Henning, Th. 2006, ApJ, 641, 838
Gratton, R. G., Carretta, E., Eriksson, K., & Gustafsson, B. 1999, A&A, 350, 955
Gratton, R. G., & Sneden, C. 1994, A&A, 287, 927
Hannaford, P., Lowe, R. M., Grevesse, N., Biemont, E., & Whaling, W. 1982, ApJ, 261, 736
Hartwick, F. D. A. 1976, ApJ, 209, 418
Hinkle, K., Wallace, L., Valenti, J., & Harmer, D. (ed.) 2000, Visible and Near Infrared Atlas of the Arcturus Spectrum 3727-9300 Å (San Francisco, CA: ASP)
Ibata, R. A., Gilmore, G., & Irwin, M. J. 1994, Natur, 370, 194
Johnson, H. L., Iriarte, B., Mitchell, R. I., & Wisniewski, W. Z. 1966, CoLPL, 4, 99
Johnson, J. A., Ivans, I. I., & Stetson, P. B. 2006, ApJ, 640, 801
Käppeler, F., Beer, H., & Wisshak, K. 1989, RPPh, 52, 945
Karakas, A. I., García-Hernández, D. A., & Lugaro, M. 2012, ApJ, 751, 8
Karakas, A. I., & Lattanzio, J. C. 2003, PASA, 20, 279
Kelson, D. D. 2003, PASP, 115, 688
Kirby, E. N., Lanfranchi, G. A., Simon, J. D., Cohen, J. G., & Guhathakurta, P. 2011, ApJ, 727, 78
Koch, A., & McWilliam, A. 2008, AJ, 135, 1551
Koch, A., & McWilliam, A. 2010, AJ, 139, 2289
Koch, A., & McWilliam, A. 2011, AJ, 142, 63
Kroupa, P., & Weidner, C. 2003, ApJ, 598, 1076
Kroupa, P., Weidner, C., Pflamm-Altenburg, J., et al. 2011, in Planets, Stars and Stellar Systems, ed. T. D. Oswalt & G. Gilmore (Dordrecht: Springer), 115
Kurucz, R. L., Furenlid, I., Brault, J., & Testerman, L. 1984, "Solar flux atlas from 296 to 1300 nm" National Solar Observatory Atlas (Sunspot, NM: National Solar Observatory)
Lamb, J. B., Oey, M. S., Graus, A. S., Adams, F. C., & Segura-Cox, D. M. 2013, ApJ, 763, 101
Lambert, D. L., Smith, V. V., Busso, M., Gallino, R., & Straniero, O. 1995, ApJ, 450, 302
Layden, A. C., & Sarajedini, A. 2000, AJ, 119, 1760
Lee, T. A. 1970, ApJ, 162, 217
Letarte, B., Hill, V., Tolstoy, E., et al. 2010, A&A, 523, 17
Lind, K., Asplund, M., Barklem, P. S., & Belyaev, A. K. 2011, A&A, 528, 103
Liu, S., Nissen, P. E., Schuster, W. J., et al. 2012, A&A, 541, A48
Lodders, K., Palme, H., & Gail, H.-P. 2009, in Abundances of the Elements in the Solar System, Landolt–Börnstein, New Series, Vol. VI/4B, Chap. 4.4, ed. J. E. Trümper (Berlin: Springer), 560
Lucatello, S., Gratton, R., Cohen, J. G., et al. 2003, AJ, 125, 875
Maeda, K., Röpke, F. K., Fink, M., et al. 2010, ApJ, 712, 624
Malaney, R. A. 1987, ApJ, 321, 832
Massey, P. 2003, ARA&A, 41, 15
Massey, P., Armandroff, T. E., Pyke, R., Patel, K., & Wilson, C. D. 1995b, AJ, 110, 2715
Massey, P., Lang, C. C., DeGioia-Eastwood, K., & Garmany, C. D. 1995a, ApJ, 438, 188
Matteucci, F., & Brocato, E. 1990, ApJ, 365, 539
McWilliam, A. 1998, AJ, 115, 1640
McWilliam, A., Matteucci, F., Ballero, S., et al. 2008, AJ, 136, 367
McWilliam, A., Preston, G. W., Sneden, C., & Searle, L. 1995, AJ, 109, 2757
McWilliam, A., & Rich, R. M. 2004, in Origin and Evolution of the Elements, ed. A. McWilliam & M. Rauch (Pasadena, CA: Carnegie Obs.), 38
McWilliam, A., Rich, R. M., & Smecker-Hane, T. A. 2003, ApJL, 592, L21
McWilliam, A., & Searle, L. 1999, Ap&SS, 265, 133
McWilliam, A., & Smecker-Hane, T. A. 2005a, in ASP Conf. Ser. 336, Cosmic Abundances as Records of Stellar Evolution and Nucleosynthesis in Honor of David L. Lambert, ed. T. G. Barnes III & F. N. Bash (San Francisco, CA: ASP), 221 (MS05)

McWilliam, A., & Smecker-Hane, T. A. 2005b, ApJL, 622, L29
Mishenina, T. V., Kovtyukh, V. V., Soubiran, C., Travaglio, C., & Busso, M. 2002, A&A, 396, 189
Monaco, L., Bellazzini, M., Ferraro, F. R., & Pancino, E. 2005, MNRAS, 356, 1396
Mottini, M., Wallerstein, G., & McWilliam, A. 2008, AJ, 136, 614
Mucciarelli, A., Carretta, E., Origlia, L., & Ferraro, F. R. 2008, AJ, 136, 375
Mucciarelli, A., Origlia, L., & Ferraro, F. R. 2010, ApJ, 717, 277
Nishimura, N., Fischer, T., Thielemann, F.-K., et al. 2012, ApJ, 758, 9
Nissen, P. E., & Schuster, W. J. 1997, A&A, 326, 751
Nissen, P. E., & Schuster, W. J. 2011, A&A, 530, A15
Nomoto, K., Thielemann, F.-K., & Yokoi, K. 1984, ApJ, 286, 644
Oey, M. S. 2011, ApJL, 739, L46
Pancino, E., Pasquini, L., Hill, V., Ferraro, F. R., & Bellazzini, M. 2002, A&A, 568, L101
Pietrinferni, A., Cassisi, S., Salaris, M., & Castelli, F. 2004, ApJ, 612, 168
Pignatari, M., Gallino, R., Heil, M., et al. 2010, ApJ, 710, 1557
Pompéia, L., Hill, V., Spite, M., et al. 2008, A&A, 480, 379
Prantzos, N., Hashimoto, M., & Nomoto, K. 1990, A&A, 234, 211
Pumo, M. L., Contino, G., Bonanno, A., & Zappalá, R. A. 2010, A&A, 524, A45
Pumo, M. L., Contino, G., Bonanno, A., & Zappalá, R. A. 2012, MSAIS, 19, 197
Raiteri, C. M., Gallino, R., Busso, M., Neuberger, D., & Kaeppeler, F. 1993, ApJ, 419, 207
Ramírez, I., & Meléndez, J. 2005, ApJ, 626, 465
Reddy, B. E., Lambert, D. L., & Allende Prieto, C. 2006, MNRAS, 367, 1329
Reddy, B. E., Tomkin, J., Lambert, D. L., & Allende Prieto, C. 2003, MNRAS, 340, 304
Reid, I. N., Gizis, J. E., & Hawley, S. L. 2002, AJ, 124, 2721
Sarajedini, A., & Layden, A. C. 1995, AJ, 109, 1086
Sarajedini, A., & Layden, A. C. 1997, AJ, 113, 264
Sbordone, L., Bonifacio, P., Buonanno, R., et al. 2007, A&A, 465, 815
Scalo, J. 2005, in The Initial Mass Function 50 Years Later, ed. E. Corbelli & F. Palle, INAF Osservatorio Astrofisico di Arcetri, Firenze, Italy; H. Zinnecker, Astrophysikalisches Potsdam, Germany (Astrophysics and Space Science Library, Vol. 327; Dordrecht: Springer), 23
Searle, L., & Sargent, W. L. W. 1972, ApJ, 173, 25
Shetrone, M. D., Côté, P., & Sargent, W. L. W. 2001, ApJ, 548, 592
Shetrone, M. D., Venn, K. A., Tolstoy, E., et al. 2003, AJ, 125, 684
Siegel, M. H., Dotter, A., Majewski, S. R., et al. 2007, ApJL, 667, L57
Simmerer, J., Sneden, C., Cowan, J. J., et al. 2004, ApJ, 617, 1091
Simmerer, J., Sneden, C., Ivans, I. I., et al. 2003, AJ, 125, 2018
Skrutskie, M. F., Cutri, R. M., Stiening, R., et al. 2006, AJ, 131, 1163
Smecker-Hane, T. A., & McWilliam, A. 2002, arXiv:astro-ph/0205411 (SM02)
Smith, V. V., Suntzeff, N. B., Cunha, K., et al. 2000, AJ, 119, 1239
Sneden, C. 1973, ApJ, 184, 839
Sneden, C., McWilliam, A., Preston, G. W., et al. 1996, ApJ, 467, 819
Sneden, C., Preston, G. W., McWilliam, A., & Searle, L. 1994, ApJL, 431, L27
Sobeck, J. S., Ivans, I. I., Simmerer, J. A., et al. 2006, AJ, 131, 2949
Tautvaišienė, G., Geisler, D., Wallerstein, G., et al. 2007, AJ, 134, 2318
The, L.-S., El Eid, M. F., & Meyer, B. S. 2000, ApJ, 533, 998
Timmes, F. X., Woosley, S. E., & Weaver, T. A. 1995, ApJS, 98, 617
Tinsley, B. M. 1979, ApJ, 229, 1046
Tolstoy, E., Venn, K. A., Shetrone, M., et al. 2003, AJ, 125, 707
Tomkin, J., & Lambert, D. L. 1999, ApJ, 523, 234
Van der Swaelmen, M., Hill, V., & Primas, F. 2012, in SF2A-2012: Proceedings of the Annual Meeting of the French Society of Astronomy and Astrophysics, ed. S. Boissier et al., 395
van Raai, M. A., Lugaro, M., Karakas, A. I., García-Hernández, D. A., & Yong, D. 2012, A&A, 540, A44
Venn, K. A., Irwin, M., Shetrone, M., et al. 2004, AJ, 128, 1177
Venn, K., Shetrone, M. D., Irwin, M. J., et al. 2012, ApJ, 751, 102
Wallerstein, G. 1962, ApJS, 6, 407
Wanjo, S., Tamamura, M., Itoh, N., et al. 2003, ApJ, 593, 968
Weidner, C., & Kroupa, P. 2005, ApJ, 625, 754
Winkler, H. 1997, MNRAS, 287, 481
Woodgate, G. K. 1980, Elementary Atomic Structure (Oxford: Oxford Univ. Press)
Woosley, S. E., & Weaver, T. A. 1995, ApJS, 101, 181
Yong, D., Aoki, W., Lambert, D. L., & Paulson, D. B. 2006, ApJ, 639, 918
Yong, D., Lambert, D. L., Paulson, D. B., & Carney, B. W. 2008, ApJ, 673, 854